UNSTABLE STATES IN LASER ASSISTED AND CONTROLLED MOLECULAR PROCESSES

O. Atabek[a], R. Lefebvre[a,b], T.T. Nguyen-Dang[c]

[a] *Institut des Sciences Moléculaires d'Orsay, Bâtiment 350, Université Paris-Sud 11 Campus d'Orsay, 91405 Orsay, France*
[b] *UFR de Physique Fondamentale et Appliquée, UPMC, 75005, Paris, France*
[c] *Département de Chimie, Université Laval, Québec, G1K 7P4, Canada*

Abstract

Many aspects of intense-field molecular dynamics rely on the concept of resonances. The chapter gives a thorough review of these aspects, bringing out the specificity of laser-induced resonances, in particular those defined in the Floquet or dressed molecule picture. The role of these resonances in the time-resolved dynamics of molecules subjected to an intense, ultrafast laser pulse is discussed and basic mechanisms of molecular fragmentation and its control are reviewed. We discuss how a thorough interpretation of two-colour XUV + IR pump-probe experiments on the dissociative ionization of H_2 can be made in terms of adiabatic vs. non-adiabatic resonance transports (*i.e.* laser-induced time evolutions) and in terms of field-induced processes such as Bond-Softening (BS) and Vibrational Trapping (VT), associated with the Floquet representation or the Dynamical Dissociation Quenching (DDQ) effects associated with a time-dependent quasi-static representation. Another application of the concepts of laser-induced resonances, and of their adiabatic evolution, is devoted to laser control strategies based on Zero-Width Resonances (ZWR) and Exceptional Points (EP), the approach of which in laser parameter space corresponds to the coalescence of two laser-induced resonances. We illustrate how the concept of ZWR can be useful for the molecular cooling problem. We then show

Email addresses: osman.atabek@u-psud.fr (O. Atabek), roland.lefebvre@u-psud.fr (R. Lefebvre), tung@chm.ulaval.ca (T.T. Nguyen-Dang)

how advantage can be taken of resonance coalescence at an EP to devise new laser control strategies pertaining to vibrational energy transfer processes.

Keywords: Resonances, Multiphoton Dissociation, Floquet Theory, Attosecond Pump-Probe Spectroscopy, Zero-Width Resonances, Exceptional Points, Laser Control, Adiabaticity, Non-Adiabatic Processes.

PACS: 33.80.Gj, 31.70.Hq, 33.90.+h, 31.50.Gh, 31.15.xv, 31.15.xg

---

Contents

1 Introduction **4**

2 General Theory of Laser-Molecule Interactions **7**

2.1 Molecular Hamiltonian in the Presence of a Laser Field 7

2.2 Multichannel Molecular Models 7

2.3 Floquet Theory 10

2.4 Dressed Molecule Picture and Laser Induced Resonances 14

2.5 Adiabatic Time Development 18

2.5.1 Adiabatic Floquet Representation: 18

2.5.2 Adiabaticity In Non-Floquet Representations: 21

3 Numerical Methodologies **22**

3.1 Time Independent Calculations of Floquet Resonances 22

3.2 Time Dependent Wavepacket Propagation 26

4 Processes and Mechanisms for Molecular Fragmentations in IR and UV-Vis Frequency Regimes **29**

4.1 General Ideas 29

4.2 A Simple Model System 30

4.3 Multiphoton Dissociation in the IR Regime 33

4.4 ATD Dynamics in the UV-Vis Regime 35

5 XUV+IR Pump-Probe Spectroscopy of Molecular Dissociative Ionization **38**

5.1 Introduction 38
5.2 Experimental context 39
5.3 Theoretical Simulations 41
5.4 Adiabatic vs. Non-adiabatic Floquet Resonance Dynamics 42

6 Zero-Width Resonances and Exceptional Points in molecular photodissociation 48

6.1 Introduction 48
6.2 Semiclassical theory 49
6.3 Zero-Width Resonances and coalescence at an Exceptional Point 51
6.4 Vibrational Purification Using ZWR 52
6.5 Vibrational transfer around an Exceptional Point 55

7 Conclusion 61

1. Introduction

The detailed description of the interactions between a molecule and a strong electromagnetic field provides the key for the interpretation of laser-induced and laser-controlled photochemical reactions [1]. Not only can structural and dynamical properties of molecules involved in such a reaction be analyzed or the nature and the role of transient species be probed, but the reaction itself can be optimally controlled by using appropriate sources of radiation. Intense laser fields apply forces to molecules that are strong enough to produce important distortions and offer the possibility to control both internal (total and partial dissociation rates as well as fragment kinetic and angular distributions) and external motions (angular positioning of the molecule with respect to the laser polarization vector). Resonances play an important part in the theoretical understanding of a wide variety of laser induced molecular processes, ranging from dynamical interpretations of photofragmentation spectra[2, 3] to the depiction of basic mechanisms used as ingredients in laser control of reactivity[4, 5, 6]. These unstable states in the molecular continuous spectra are characterized by quantized complex energies, resulting from their outgoing asymptotic behavior (Siegert boundary conditions[7]). Their imaginary parts are inversely proportional to their lifetimes. Several techniques have so far been developed for their accurate calculation by solving close-coupled differential equations, with appropriate boundary conditions[4, 8]. In the context of intense laser fields, these equations describe nuclear motions on multiphoton field-dressed electronic potentials of the Floquet Hamiltonian[2, 3, 9]. Such laser induced potentials, apart from accommodating resonances, also lead to a clear understanding of basic mechanisms. Among them, bond softening or vibrational trapping in the Above Threshold Dissociation (ATD) regime[3], acting in an antagonistic manner[5], open the way to efficient and robust control scenarios (reactivity, alignment/orientation, purification, vibrational transfer). These mechanisms have experimentally confirmed counterparts in the time domain and may considerably affect the wave packet dynamics when referring to short pulse durations:

barrier lowering and Dynamical Dissociation Quenching (DDQ)[10, 11, 12],[13].

Highly-nonlinear field-induced barrier lowering or suppression and stabilization (trapping or quenching) mechanisms both in the Visible-Ultra-Violet (Vis-UV)[3] and the Infra-Red (IR)[10, 11, 12] frequency regimes underly chemical bond softening or hardening processes, respectively. Their interplay through the adequate adjustment of laser characteristics such as laser frequency, amplitude, phase, polarization, and temporal shape, provides interesting novel control opportunities[5]. In the presence of strong fields, resonances also show highly non-linear features. The widths increase with the field intensity in a non-perturbative way (in the cases of shape resonances) but, in some circumstances and more unexpectedly, they may saturate and even decrease (the cases of Feshbach resonances). The decrease is such that for some values of the laser parameters (frequency and intensity) one can reach strictly zero width, a counterintuitive situation where a molecule irradiated by a strong field becomes stable. A so called bound state in a continuum or a Zero-Width Resonance (ZWR) is obtained[14, 6]. For other choices of field parameters, one can realize a coalescence of two resonances, one of the shape type, the other of Feshbach type, as a so-called Exceptional Point (EP)[15] is reached[16]. ZWRs and EPs lead to very interesting control issues, involving molecular cooling and vibrational population transfer strategies[6, 16].

The present chapter reviews these aspects of intense-field molecular dynamics and discusses their pertinence to the detailed interpretation of two-colour dissociative ionization experiments and the laser-control theory. The chapter is organized as followed. The theory of laser-molecule interactions is presented in Section 2, starting from a general multicharged system considered in a semiclassical field description. The Hamiltonian of the laser-driven system is given in the length gauge[1, 17, 18, 19]. The Section continues with a thorough analysis of multichannel field-dressed molecular models within the Born-Oppenheimer approximation[20] (for the molecular part) and the Floquet formalism[9, 21] (for the radiative part). Section 3 is devoted to numerical methodologies for solving coupled equations describing the dynamics of a laser-driven two-channel

(two-electronic-state) molecule, either in a time independent frame, where emphasis is placed on field-induced resonances, or in a time dependent context, highlighting time-resolved features. Basically, the numerical techniques that are retained are the Fox-Goodwin propagator[8] using complex rotation[22] of the spatial coordinate (time independent approach), or the split-operator formula coupled to Fast Fourier Transform algorithms[23] adequately modified to take advantage of Volkov type solutions[24] in asymptotic regions (time dependent approach). Dynamical processes with their underlying mechanisms and control strategies are presented in Section 4.

As a first application of the theory, concepts and methodologies of sections 2 and 3, we discuss the dissociative ionization dynamics of the molecular ion H_2^+ under two-colour XUV + IR pump-probe ultrafast, intense laser excitations. In Section 5 the results of wavepacket dynamics simulations, done within a theory/experiment collaboration[25, 26], are compared to experimental data, aiming at a thorough interpretation in terms of resonances and basic mechanisms. In one series of experiments using IR pulses that are shorter than the vibrational period of H_2^+, de-phasing and re-phasing of the vibrational wave packet that is formed in H_2^+ upon ionization of the neutral molecule by the XUV pulse are observed. This observation is interpreted in terms of a laser-molecule synchronization similar to that of the DDQ mechanism[10]-[12]. In experiments where the duration of the IR pulse exceeds the vibrational period of H_2^+, a pronounced dependence of the H^+ kinetic energy distribution on XUV-IR delay is observed, that can be explained in terms of the adiabatic propagation of the H_2^+ wave packet and the bond-softening mechanism on field-dressed potential energy curves.

The second application, considered in Section 6, is devoted to laser control strategies based on Zero-Width Resonances and Exceptional Points[27]. A semiclassical model helps in determining, for a given wavelength, the laser intensity at which a ZWR is produced. The ZWR is shown to be useful for vibrational purification processes and thus ultimately for molecular cooling control. Finally, it is also shown how an appropriate choice of laser parameters may provoke the

approach of an Exceptional Point leading to the coalescence of two resonances (complex eigenenergies and wavefunctions). We show how advantage can be taken of such a situation in devising innovative laser control strategies pertaining to vibrational energy transfer processes.

2. General Theory of Laser-Molecule Interactions

2.1. Molecular Hamiltonian in the Presence of a Laser Field

Many forms of the Hamiltonian operator describing a system interacting with a radiation field are currently in use[18, 19, 1, 4]. These are defined within either of two descriptions: One is fully quantized and treats both the laser field and the molecular system quantum mechanically. The other is semiclassical and assumes at the outset a classical field while the charged particles are treated quantum mechanically. We recall here the expression of the Hamiltonian of a laser-driven molecule written in the semiclassical description; this will serve to lay the ground work for the construction of the models encountered in the subsequent Sections. It is to be recalled also that many equivalent forms of the radiative interaction exist, corresponding to different choices of the electromagnetic field's gauge. We will systematically refer to the so-called Coulomb length-gauge in writing the interaction between a charged particle of a molecule and a radiation field. Also, only electric dipole interactions are considered within the so-called long-wavelength approximation.

2.2. Multichannel Molecular Models

For a complete treatment of a laser-driven molecule, one must solve the many-body, multidimensional TDSE. This represents a tremendous task and direct wavepacket simulations of nuclear and electronic motions under an intense laser pulse is presently restricted to a few bodies (at most three or four) and/or to a model of low dimensionality[28]. For a more general treatment, an approximate separation of variables between electrons (fast subsystem) and nuclei (slow subsystem) is customarily made, in the spirit of the Born-Oppenheimer

approximation. To lay out the ideas underlying this approximation as adapted to field-driven molecular dynamics, we will consider from now on a molecule consisting of N_n nuclei (labeled $\alpha, \beta...$) and N_e electrons (labeled $i, j, ...$), with position vectors $\mathbf{R}_\alpha$ and $\mathbf{r}_i$ respectively, defined in the center of mass (rotating) body-fixed coordinate system, in a classical field $\mathbf{E}(t)$ of the form $\mathbf{E}_0 f(t)\cos(\omega t)$. The full semiclassical length-gauge Hamiltonian is written, for a system of electrons and nuclei, as[4]:

$$H(t) = H_{el}(t) + T_N - \boldsymbol{\mu}_N(\{\mathbf{R}_\alpha\}) \cdot \mathbf{E}(\mathbf{t}) \tag{2.1}$$

with:

$$H_{el}(t) = \sum_i \frac{\mathbf{p}_i^2}{2m} + V(\{\mathbf{r}_i\}, \{\mathbf{R}_\alpha\}) + e\sum_i \mathbf{r}_i \cdot \mathbf{E}(t) \tag{2.2}$$

where T_N denotes the kinetic energy and $\boldsymbol{\mu}_N(\{\mathbf{R}_\alpha\}$ is the dipole moment operator associated with the nuclei. This gauge has the advantage of giving a simple form for the close-coupled equations, as is clarified hereafter.

In the electronic Hamiltonian $H_{el}(t)$, the potential function $V(\{\mathbf{r}_i\}, \{\mathbf{R}_\alpha\})$ comprises all Coulomb interactions between the charges, i.e. it is the sum of V_{en}, the attraction between electrons and nuclei, V_{ee}, the Coulomb repulsion between the electrons, as well as V_{nn}, the repulsion between the various nuclei of the molecular system. The sum of $V(\{\mathbf{r}_i\}, \{\mathbf{R}_\alpha\})$ and the electronic kinetic energy defines the field-free electronic Hamiltonian, H_{el}^0:

$$H_{el}^0 = \sum_i \frac{\mathbf{p}_i^2}{2m} + V(\{\mathbf{r}_i\}, \{\mathbf{R}_\alpha\}). \tag{2.3}$$

Its eigenfunctions,

$$H_{el}^0 \Xi_I(\{\mathbf{r}_i\}; \{\mathbf{R}_\alpha\}) = \epsilon_I(\{\mathbf{R}_\alpha\})\Xi_I(\{\mathbf{r}_i\}; \{\mathbf{R}_\alpha\}), \tag{2.4}$$

which are supposedly orthonormal by construction, constitute a complete basis in terms of which the total molecular wavefunction can be expanded:

$$\Omega(\{\mathbf{r}_i\}, \{\mathbf{R}_\alpha\}, t) = \sum_I \Psi_I(\{\mathbf{R}_\alpha\}, t)\Xi_I(\{\mathbf{r}_i\}; \{\mathbf{R}_\alpha\}). \tag{2.5}$$

It is to be noted that the dependence of the electronic basis wavefunctions $\Xi_I(\{\mathbf{r}_i\}; \{\mathbf{R}_\alpha\})$ on the nuclear coordinates $\{\mathbf{R}_\alpha\}$ is a parametric one. Since

the field-free electronic Hamiltonian is time independent, the basis set is independent of time. Yet, the expansion coefficients $\Psi_I(\{\mathbf{R}_\alpha\}, t)$ in this basis are time-dependent and have to obey the reduced coupled Schrödinger equations:

$$i\hbar\frac{\partial\Psi_I(\{\mathbf{R}_\alpha\},t)}{\partial t} = [T_N + \epsilon_I(\{\mathbf{R}_\alpha\}) - \boldsymbol{\mu}_N(\{\mathbf{R}_\alpha\})\cdot\mathbf{E}(t)]\,\Psi_I(\{\mathbf{R}_\alpha\},t)$$
$$- \quad \mathbf{E}(t)\cdot\sum_J\langle\Xi_I|(-e\sum_i\mathbf{r}_i)|\Xi_J\rangle\Psi_J(\{\mathbf{R}_\alpha\},t) + \sum_J\mathcal{C}_{I,J}\Psi_J(\{\mathbf{R}_\alpha\},t), \quad (2.6)$$

where $\mathcal{C}_{I,J}$ are non-adiabatic coupling operators, the exact form of which depends on the choice of nuclear coordinates. When the field is turned off, (i.e. $\mathbf{E}(t) = 0$), neglect of the non-radiative (*i. e.*non-adiabatic) coupling terms on the third line of this equation yields the celebrated Born-Openheimer (BO) approximation[20]: Since no coupling then exists any longer between the various Ψ_I's, the expansion of Eq. (2.5) reduces to a single term denoting an approximate separation of nuclear and electronic variables. While the electronic part is described by Eq. (2.4), an effective Schrödinger equation describes the nuclear motions viewed as occurring on a single potential energy surface (PES), a single *electronic channel*, described by the electronic energy $\epsilon_I(\{\mathbf{R}_\alpha\})$ which now plays the role of a potential energy function. In field-free molecular dynamics, the neglect of non-adiabatic couplings is usually justified, at least in part, by the disparity between the nuclear and the electronic masses. Here, their neglect is justified by the observation that they are dominated by the strong couplings between the electronic states or *channels* as induced by the intense laser field. Thus neglecting these non-radiative couplings (the last sum in Eq. (2.6)) to concentrate on field-induced effects, we obtain

$$i\hbar\frac{\partial\Psi_I(\{\mathbf{R}_\alpha\},t)}{\partial t} = [T_N + \epsilon_I(\{\mathbf{R}_\alpha\}) - \boldsymbol{\mu}_N(\{\mathbf{R}_\alpha\})\cdot\mathbf{E}(t)]\,\Psi_I(\{\mathbf{R}_\alpha\},t)$$
$$-\mathbf{E}(t)\cdot\sum_J\langle\Xi_I|(-e\sum_i\mathbf{r}_i)|\Xi_J\rangle\Psi_J(\{\mathbf{R}_\alpha\},t). \quad (2.7)$$

This is the start of the construction of multichannel models of laser-driven molecules. In practice, one restricts to a finite number, N_{ch}, of electronic states, selected on the basis of physical relevance and Eq. (2.7) defines an N_{ch}-channel molecular model system. The 'electronic' Hamiltonian is, in this model, de-

scribed by the operator

$$H_{el}(\{\mathbf{R}_\alpha\},t)=\sum_{I,J}[\epsilon_I(\{\mathbf{R}_\alpha\})\delta_{IJ}-\mathbf{E}(t)\cdot\boldsymbol{\mu}_{IJ}(\{\mathbf{R}_\alpha\})]|\mathbf{\Xi_I}\rangle\langle\mathbf{\Xi_J}|, \tag{2.8}$$

where

$$\boldsymbol{\mu}_{IJ}(\{\mathbf{R}_\alpha\})=\langle\Xi_I|(-e\sum_i\mathbf{r}_i)|\Xi_J\rangle \tag{2.9}$$

is the transition dipole moment between the field-free electronic states $\mid\Xi_I\rangle$ and $\mid\Xi_J\rangle$. In matrix form, H_{el} is represented by

$$\tilde{\mathbf{W}}(\{\mathbf{R}_\alpha\};t)=\begin{pmatrix}\epsilon_1-\boldsymbol{\mu}_{11}\cdot\mathbf{E}(t) & -\boldsymbol{\mu}_{12}\cdot\mathbf{E}(t) & .. & .. & ..\\ -\boldsymbol{\mu}_{21}\cdot\mathbf{E}(t) & \epsilon_2-\boldsymbol{\mu}_{22}\cdot\mathbf{E}(t) & -\boldsymbol{\mu}_{23}\cdot\mathbf{E}(t) & .. & ..\\ .. & -\boldsymbol{\mu}_{32}\cdot\mathbf{E}(t) & \epsilon_3-\boldsymbol{\mu}_{33}\cdot\mathbf{E}(t) & -\boldsymbol{\mu}_{34}\cdot\mathbf{E}(t) & ..\\ .. & .. & .. & .. & ..\end{pmatrix} \tag{2.10}$$

and, gathering the nuclear amplitudes $\Psi_I(\{\mathbf{R}_\alpha\},t)$ into a column vector $\mathbf{\Psi}(\{\mathbf{R}_\alpha\},t)$, Eq. (2.7) reads:

$$i\hbar\frac{\partial\mathbf{\Psi}(\{\mathbf{R}_\alpha\},t)}{\partial t}=\left[T_N\mathbf{1}+\tilde{\mathbf{W}}(\{\mathbf{R}_\alpha\};t)\right]\mathbf{\Psi}(\{\mathbf{R}_\alpha\},t). \tag{2.11}$$

2.3. Floquet Theory

When the external field is a continuous wave (cw) field,

$$\mathbf{E}(t)=\mathbf{E}_0\cos\omega t \tag{2.12}$$

the various Hamiltonians given above, in eq.(2.1), (2.2) or in eq.(2.11), are time-periodic of period $T=2\pi/\omega$, i.e. $H(t+T)=H(t)$. Owing to this time-periodicity, the Floquet theorem[21] is applicable to the TDSE associated with that Hamiltonian. We recall here the main concepts of Floquet theory as applied to the Schrödinger equation

$$i\hbar\frac{\partial\mid\Psi(t)\rangle}{\partial t}=H(t)\mid\Psi(t)\rangle, \tag{2.13}$$

for any of the time-periodic Hamiltonians refered to above (specialization to a specific form of this Hamiltonian will be made later). Floquet theorem states that this TDSE admits solutions of the form:

$$\mid\Psi_E(t)\rangle=e^{-i\frac{Et}{\hbar}}\mid\Phi_E(t)\rangle, \tag{2.14}$$

with $\mid \Phi_E(t+T)\rangle = \mid \Phi_E(t)\rangle$, which constitute a complete basis for a full description of the dynamics[1]. Introduction of the Floquet form into the wave equation produces for $\mid \Phi_E(t)\rangle$ the equation:

$$[H(t) - i\hbar\frac{\partial}{\partial t}] \mid \Phi_E(t)\rangle = E \mid \Phi_E(t)\rangle. \tag{2.15}$$

The operator acting on $\mid \Phi_E(t)\rangle$ is called the Floquet Hamiltonian,

$$H_F(t) = H(t) - i\hbar\frac{\partial}{\partial t}, \tag{2.16}$$

and the time in this is to be treated as an additional dynamical variable so that Eq. (2.15) determines eigenvalues and eigenstates of the Floquet Hamiltonian in an extended space, the direct product of the usual molecular Hilbert space and the space of periodic functions of $t \in [0, T]$. This extension of the Hilbert space can be made somewhat more transparent by introducing a new time-like variable, to be distinguished from the actual time variable t. This new time variable can be defined through the arbitrary phase of the continuous (periodic) field, as done in [29, 30]. A variant of the idea is found in the (t,t′) method developped by Moiseyev *et al.* [31] and applied to the photodissociation of H_2^+ [32, 33]. We will continue with the more traditional and simpler formulation of Floquet theory here, as this is sufficient to bring out ideas of laser-induced resonances in the dressed molecule picture.

In all strong-field molecular dynamics problems, the Hamiltonian $H(t)$ can be split into a time independent part, denoting the field-free molecule, and a time dependent one representing the matter-field interaction:

$$H(t) = H_0 + V(t). \tag{2.17}$$

The time-periodic part $\mid \Phi_E(t)\rangle$ of the Floquet eigenvector and the time dependent interaction 'potential'[2] $V(\mathbf{r}, \mathrm{t})$ can be written in the form of a discrete

[1] The theorem applies to scattering and bound states with a real energy and to resonance states with a complex energy. When the energy is quantized (bound and resonance states), it is called a quasi-energy, for reasons to be developped below.

[2] To fix the idea, we shall henceforth consider the case this interaction term depends on $\mathbf{r}$, as in the length gauge Hamiltonian.

Fourier series,

$$V(\mathbf{r},t) = \sum_n V_n(\mathbf{r}) e^{in\omega t}, \tag{2.18}$$

and:

$$\mid \Phi_E(t)\rangle = \sum_n \mid U_n\rangle e^{in\omega t} \tag{2.19}$$

with n going from $-\infty$ to $+\infty$. In the case of eq.(2.19) for the Floquet wavefunction $\mid \Phi_E(t)\rangle$, we are in fact expanding it in the complete orthonormal basis of periodic function of the new dynamical variable t, $e^{in\omega t}$. Substituting these expansions into the Floquet eigenvalue equation (Eq. (2.15)) results in an elimination of the time variable to give a system of coupled *time independent* equations:

$$[H_0 + V_0(\mathbf{r})] \mid U_n\rangle + \sum_{n' \neq n} V_{n-n'}(\mathbf{r}) \mid U_{n'}\rangle = (E - n\hbar\omega) \mid U_n\rangle. \tag{2.20}$$

In the case of a matter-field interaction of the form

$$V(\mathbf{r},t) = -\boldsymbol{\mu}(\mathbf{r}) \cdot \mathbf{E}(t) = -\frac{1}{2}\boldsymbol{\mu}(\mathbf{r}) \cdot \mathbf{E}_0[e^{i\omega t} + e^{-i\omega t}], \tag{2.21}$$

as found in Eqs.(2.1) and (2.2) with a cosine electric field, $V(t)$ has only two non-zero Fourier components:

$$V_{\pm 1} = -\frac{1}{2}\boldsymbol{\mu}(\mathbf{r}) \cdot \mathbf{E}_0 \tag{2.22}$$

so that the coupled equations (2.20) reduce to

$$(H_0 + n\hbar\omega) \mid U_n\rangle - \frac{1}{2}\boldsymbol{\mu}(\mathbf{r}) \cdot \mathbf{E}_0(\mid U_{n+1}\rangle + \mid U_{n-1}\rangle) = E \mid U_n\rangle \tag{2.23}$$

A number of basic properties of the Floquet states $\mid \Psi_E(t)\rangle$ can be infered easily from Eqs (2.14) and (2.19). First, if E_i is a quasi-energy, i.e. an eigenvalue of H_F associated with an eigenstate $\mid \Phi_{E_i}(t)\rangle$, then

$$E_{i,k} = E_i + k\hbar\omega. \tag{2.24}$$

is also an eigenvalue, i.e. it also belongs to the Floquet energy spectrum. The eigenvector associated with this eigenvalue is obtained by multiplying $\mid \Phi_{E_i}(t)\rangle$

with $e^{ik\omega t}$ as can be verified by substituting the new periodic function $e^{ik\omega t} \mid \Phi_{E_i}(t)\rangle$ into Eq. (2.19). Accordingly, the Fourier indices n labeling the components $\mid U_n\rangle$ are shifted by $-k$, i.e $\mid U_n^{E+k}\rangle = \mid U_{n-k}^{E}\rangle$. Thus quasi-energies are defined modulo an integer multiple of $\hbar\omega$, and should therefore be identified by at least two indices, as evoked in Eq. (2.24): Together with i, the index k defines a quasi-energy level in a definite Brillouin zone, which is specified by k alone. This is in complete analogy with the situation met in crystals, where the Floquet theorem also applies, but this time as a result of the spatial periodicity of the potential, and is called Bloch theorem[34]. It is known that the Floquet states belonging to a single zone constitute a complete basis set[35], in the case where the quasi-energy spectrum is discrete. Extension to cases involving continua and resonance states can be made heuristically by invoking a continuum discretization procedure.

Second, the properties of Floquet eigenstates are such as to produce a very simple *stroboscopic* way of following the motion of a general wave-packet of the time dependent laser-driven system: Consider the evolution operator $\mathcal{U}(t+T,t)$ between times t and $t+T$. Starting at time t from a Floquet state

$$\mid \Psi_i(t)\rangle = e^{-i\frac{E_i t}{\hbar}} \mid \Phi_i(t)\rangle, \tag{2.25}$$

we have after time T:

$$\mathcal{U}(t+T,t) \mid \Psi_i(t)\rangle = e^{-i\frac{E_i(t+T)}{\hbar}} \mid \Phi_i(t+T)\rangle = e^{-i\frac{E_i(t+T)}{\hbar}} \mid \Phi_i(t)\rangle. \tag{2.26}$$

In particular if $t = 0$:

$$\mathcal{U}(T,0) \mid \Psi_i(0)\rangle = e^{-i\frac{E_i T}{\hbar}} \mid \Phi_i(T)\rangle = e^{-i\frac{E_i T}{\hbar}} \mid \Phi_i(0)\rangle. \tag{2.27}$$

This shows that the time evolution is exactly like that of a stationary state of a time independent Hamiltonian, provided the probing is limited to T, or any multiple of T. Since $\mid \Psi_i(0)\rangle$ is equal to $\mid \Phi_i(0)\rangle$, Eq. (2.27) also shows that $\exp(-iE_iT/\hbar)$ is an eigenvalue of the evolution operator over one period of the field. Suppose now that we wish to follow the development in time of an arbitrary initial wave packet $\mid \eta(0)\rangle$. We can expand it over the complete set of

Floquet eigenfunctions of a given Brillouin zone at time $t = 0$:

$$\mid \eta(0)\rangle = \sum_i \mid \Phi_i(0)\rangle\langle\Phi_i(0) \mid \eta(0)\rangle. \tag{2.28}$$

At time $t = NT$, the wave packet has evolved into:

$$\mid \eta(NT)\rangle = \sum_i e^{-i\frac{E_i NT}{\hbar}} \mid \Phi_i(0)\rangle\langle\Phi_i(0) \mid \eta(0)\rangle. \tag{2.29}$$

This relation emphasizes again the similarity between the properties of Floquet eigenfunctions and the ordinary stationary eigenfunctions (see [36] for more details). Although it has been proven here only for stroboscopic times, Eq. (2.29) may be written more generally by changing NT into an arbitrary t.

2.4. Dressed Molecule Picture and Laser Induced Resonances

Without the coupling term linear in $\boldsymbol{\mu}$ in Eq. (2.23), the components $\mid U_n\rangle$ would solely be governed by the field-free Hamiltonian H_0 augmented by $n\hbar\omega$, the energy of n-photon. One can take Eq. (2.23) as defining the dressed molecule picture within this semiclassical description, and $\mid U_n\rangle$ is the amplitude (wavefunction) of the n-photon dressed (diabatic) channel. The field interaction $(1/2)\boldsymbol{\mu}(\mathbf{r})\cdot\mathbf{E}_0$ couples these diabatic channel amplitudes together. Diagonalizing the potential part of the full Floquet Hamiltonian matrix defined by Eq. (2.23), i.e. containing these diabatic-channel couplings, one gets an equivalent picture, called the adiabatic Floquet scheme, with channel crossings in the diabatic representation becoming avoided crossings where adiabatic amplitudes $\mid U_n^{(adia)}\rangle$ are now coupled together by strongly localized field-induced non-adiabatic couplings.

To illustrate the above concepts, we consider a two-electronic-state molecular model system, corresponding to keeping just two terms in the sum on the right-hand side (rhs) of Eq.(2.5), so that $\boldsymbol{\Psi}(\{\mathbf{R}_\alpha\}, t)$ in Eq.(2.11) is a two-dimensional column vector and $\tilde{\mathbf{W}}(\{\mathbf{R}_\alpha\}; \mathbf{t})$, a (2×2) matrix. A representative of this class of models is the one-electron diatomic H_2^+ molecule described in a two-electronic-state approximation.

Using the notations defined in Section (2.2), the position vectors in the center of mass frame of the two nuclei in this specific case are $\mathbf{R}_1 = +\mathbf{R}/2$, $\mathbf{R}_2 = -\mathbf{R}/2$, where $\mathbf{R}$ is the relative position vector, and considering the system in interaction with a linearly polarized field, the full molecular Hamiltonian for this one-electron system is:

$$H(t) = H_{el}^0 + T_N + eE_0 \cos(\omega t)\boldsymbol{\epsilon} \cdot \mathbf{r} \tag{2.30}$$

with H_{el}^0 defined by

$$H_{el}^0 = \frac{\mathbf{p}^2}{2m} + V(\mathbf{r}, \mathbf{R}), \tag{2.31}$$

$V(\mathbf{r}, \mathbf{R})$ being the sum of Coulomb interactions among the three particules. The two relevant electronic states of the H_2^+ molecule are the ground state of symmetry $^2\Sigma_g^+$, described by the wavefunction

$$\Xi_1(\mathbf{r}, \mathbf{R}) \;=\; 1s\sigma_g(\mathbf{r}, \mathbf{R}), \tag{2.32}$$

and the first excited state that is accessible via an electronic dipole allowed transition, of symmetry $^2\Sigma_u^+$, and described by[3]

$$\Xi_2(\mathbf{r}, \mathbf{R}) \;=\; 2p\sigma_u(\mathbf{r}, \mathbf{R}). \tag{2.33}$$

The $\mathbf{R}$-dependent electronic energies of these two states are noted $\epsilon_g(R)$ and $\epsilon_u(R)$. Note that, if the z axis of the molecule-fixed center of mass coordinate system is chosen to lie along the internuclear axis, then these depend explicitly on $R = |\mathbf{R}|$ only, as indicated. The time dependent statefunction $\Omega^L(\mathbf{r}, \mathbf{R}, t)$ of the system expanded in the truncated basis of the two electronic wave functions is then

$$\Omega^L(\mathbf{r}, \mathbf{R}, t) = \Psi_1(\mathbf{R}, t)\Xi_1(\mathbf{r}, \mathbf{R}) + \Psi_2(\mathbf{R}, t)\Xi_2(\mathbf{r}, \mathbf{R}). \tag{2.34}$$

With this two-component state, applying the Floquet ansatz consists of writing

$$\begin{pmatrix} \Psi_1(\mathbf{R}, t) \\ \Psi_2(\mathbf{R}, t) \end{pmatrix} = e^{-i\frac{Et}{\hbar}} \begin{pmatrix} \Phi_1(\mathbf{R}, t) \\ \Phi_2(\mathbf{R}, t) \end{pmatrix} \tag{2.35}$$

[3]Note that in designating the molecular orbitals representing these two electronic states as above, the $1s$ and $2p$ symbols refer to the united-atom limit.

and the general Floquet eigenvalue equation (2.15) takes on the following particular form

$$\begin{aligned} i\hbar\frac{\partial\Phi_1(\mathbf{R},t)}{\partial t} &= [T_N+\epsilon_g(R)-E]\Phi_1(\mathbf{R},t)-E_0\mu_{gu}(R)\cos\theta\cos(\omega t)\Phi_2(\mathbf{R},t) \\ i\hbar\frac{\partial\Phi_2(\mathbf{R},t)}{\partial t} &= [T_N+\epsilon_u(R)-E]\Phi_2(\mathbf{R},t)-E_0\mu_{ug}(R)\cos\theta\cos(\omega t)\Phi_1(\mathbf{R},t) \end{aligned} \tag{2.36}$$

where θ is the angle between the molecular internuclear axis and the direction of the polarization vector $\boldsymbol{\epsilon}$ and $\mu_{gu}(R)$ is the matrix element:

$$\mu_{gu}(R)=\langle\Xi_1(\mathbf{r},\mathbf{R})|(-ez)|\Xi_2(\mathbf{r},\mathbf{R})\rangle_{\mathbf{r}}=\mu_{ug}(R). \tag{2.37}$$

defined in the body-fixed system. The subscript $\mathbf{r}$ is to recall that the integration implied in this matrix element is made only over the electronic coordinates. Note that diagonal matrix elements of $-ez$ vanish for a homonuclear system such as H_2^+, owing to the inversion symmetry of the field-free molecule. We note that, in a complete treatment of the laser-driven dynamics, the relative nuclear kinetic energy operator T_N in Eq.(2.36) is the sum of a radial and an angular parts, $\mathbf{T}_R$, $\mathbf{T}_{\theta,\varphi}$, respectively as exhibited and defined in Eqs.(3.17)-(3.19). However, the essential features of the Floquet representation of this two-state system are best illustrated by considering a one-dimensional, rotationless molecule, for which $T_N=\mathbf{T}_R$ and $\cos\theta=1$ corresponding to the situation of a perfect alignment of the molecular axis along the laser polarization. We will briefly discuss the role of rotations,*i. e.* of angular dynamics within this Floquet scheme in section 4.

Returning to Eq.(2.36), each of the functions $\Phi_k(\mathbf{R},t),\quad k=1,2$, being time-periodic, it is expressible in the form

$$\Phi_k(\mathbf{R},t)=\sum_{-\infty}^{+\infty}e^{in\omega t}\Psi_{k,n}(\mathbf{R}), \tag{2.38}$$

corresponding to the general Eq.(2.19), i.e. $\Psi_{k,n},\ k=1,2$, are the two components of $\mid U_n\rangle$ in the two-state field-free electronic basis. Introduction of these developments into the above coupled equations (2.36) leads to:

$$[T_N+\epsilon_g(R)+n\hbar\omega]\,\Psi_{1,n}-\frac{E_0}{2}\mu_{gu}(R)[\Psi_{2,n-1}+\Psi_{2,n+1}]=E\Psi_{1,n}$$

$$[T_N + \epsilon_u(R) + n\hbar\omega]\,\Psi_{2,n} - \frac{E_0}{2}\mu_{gu}(R)[\Psi_{1,n-1} + \Psi_{1,n+1}] = E\Psi_{2,n} \qquad (2.39)$$

This pair of equations, which in fact represents an infinite set of coupled equations as n varies from $-\infty$ to $+\infty$, corresponds to the general Eq. (2.23). In this specific case, the radiative couplings follow a parity selection rule that arises from the fact that $\mu_{kk} = 0,\ k = 1, 2 \leftrightarrow g, u$, in the model considered here. Once a parity of the Fourier indices ('numbers of photons') n associated with channel 1 is chosen, the nuclear amplitudes $\Psi_{1,n}$ supported by this channel (dressed by 'n photons') are coupled only to amplitudes $\Psi_{2,n'}$ supported by channel 2 with a number n' of opposite parity. The type of dressed picture that emerges from this is illustrated in Fig. 4.2, for the dressing by a $\lambda = 532\ nm$ field of a rotationless two-state H_2^+ molecule, with even values of n associated with channel 1, and odd ones with channel 2. The corresponding R-dependent channel energies, i.e. $\epsilon_g(R)$ and $\epsilon_u(R)$, dressed by $n\hbar\omega$ according to this n-parity convention, exhibit, at specific R, crossings with $|\Delta n| = 1, 3, 5, ..$ that have been interpreted as corresponding to local electronic transitions ${}^2\Sigma_g \longrightarrow {}^2\Sigma_u$ with absorption of $1, 3,\ 5, ...$ photons respectively.

If we ignore the nuclear kinetic operator T_N in Eq. (2.39), then the resulting equation defines Floquet eigenstates of the two-state electronic system considered at a fixed R. These local electronic Floquet eigenstates and energies can thus be obtained simply by diagonalizing the local electronic Floquet Hamiltonian matrix. The results are shown in dashed lines on Fig. 4.2. Doing this leaves the problem of determining the full molecular Floquet states unsolved however, as the electronic Floquet Hamiltonian matrix and its eigenvectors do not commute with the nuclear kinetic energy operator. At best, the local electronic Floquet eigenvectors can be taken as a new basis, an adiabatic one, on which the total molecular Floquet states can be expanded. The channel amplitudes in this basis are coupled by kinetic non-adiabatic couplings, arising from the commutator between T_N and $H_F^{el}(R)$.

The dressed channels represented by the potentials traced in solid lines in Fig. 4.2 are coupled to each other by diabatic couplings that increase linearly

with E_0, i.e. with the field intensity, and that are also delocalized in R, as, for H_2^+, μ_{gu} diverges as $R/2$. In contrast, non-adiabatic couplings in the dressed adiabatic picture decrease as E_0 increases, and are localized in the neighbourhood of avoided crossings created at the one-, three-, five-,.., photon crossings of the diabatic dressed scheme. This confers to the adiabatic representation some advantages in interpretations, i.e. in the qualitative readings of calculated dynamics. In particular, laser-induced resonances, i.e. metastable Floquet states, of two sorts can clearly be identified on the adiabatic dressed potential energy curves of Fig. 4.2. These are defined by the avoided crossing created at the intersection of the $\epsilon_g + n\hbar\omega$ and the $\epsilon_u + (n-1)\hbar\omega$ curves, for any n, i.e. the one-photon crossing. The lower of the pair of adiabatic potentials associated with this avoided crossing supports resonances of shape type, while the upper one supports resonances of Feschbach type.

Shape resonances are responsible for the so-called Bond-Softening dissociation process for resonances lying below the barrier created at the one-photon crossing, and for Above-The-Barrier dissociation in the opposite situation. Feshbach resonances give rise to the Vibrational Trapping phenomenon, also called Bond-Hardening process. The positions and the widths of these resonances vary with the field intensity. In particular, the widths of shape and Feshbach resonances vary in opposite directions as the field strength increases: While shape resonances become more and more unstable, the barrier to dissociation of the lower adiabatic potential being lowered with increasing E_0, Feshbach resonances are stabilized in the same conditions, as non-adiabatic couplings that are responsible for their decays into the continua in which they are embedded are lowered as E_0 increases.

2.5. Adiabatic Time Development

2.5.1. Adiabatic Floquet Representation:

Rigorously, the above Floquet representation is valid only when the field is periodic. Imagine now that the field amplitude $\mathbf{E}_0$ in Eq.(2.12) carries a time dependence that denotes a slow modulation of the cosine field which oscillates with

a frequency ω in the UV-Vis spectral range. Without the amplitude modulation, the dynamics under the UV-Vis field is well captured by the Floquet representation. If the amplitude modulation is slow, the Floquet ansatz can still be applied to the TDSE with this locally periodic field, albeit approximately. This can be seen as followed: Within some time interval $[\bar{t}-\Delta t, \bar{t}+\Delta t],\ \Delta t = T_L/N$ around $\bar{t}$, ($T_L = 2\pi/\omega$ is the laser-field frequency), with N large enough so that the variations of the pulse enveloppe over $2\Delta t$ can be neglected, but still ensuring that some oscillations of the high frequency carrier wave do occur during that time-interval, the laser field $\mathbf{E}(t)$ can be considered of constant amplitude, i.e. it can be written $\mathbf{E}(t) = \overline{\mathbf{E}}_0 \cos\omega t$ with $\overline{\mathbf{E}}_0 := \mathbf{E}_0(\bar{t})$. The eigenstates of the instantaneous Floquet Hamiltonian $H_F^{\{\bar{t}\}}(t) = H^{\{\bar{t}\}}(t) - i\hbar\frac{\partial}{\partial t}$ associated with this local periodic field defines a basis for the expansion of the actual wavepacket of the system as it evolves during this time-interval from some initial condition. If this initial condition, which is nothing else than the wavepacket evolved up to time $\bar{t} - \Delta t$, projects unitarily, (or at least mainly) on a single state of this local basis, i.e. a single Floquet state, then it will remain in this state during the whole time-interval. Imagine now that the laser pulse duration is divided up into N_t time slices of width Δt_n centered on $\bar{t} = t_n$, $n = 0, 1, 2, ...N_t$. If the actual time-evolution across the full pulse width is essentially the transport of a single Floquet resonance state or a group of quasi-degenerate Floquet states from one time-slice to another, then the Floquet dynamics is said adiabatic. This definition represents the extension, to Floquet states, of the concept of adiabatic transport of eigenstates of time-dependent Hamiltonian as expressed by the celebrated adiabatic theorem[37]. Its precise formulation within Floquet theory has been given in different forms by many authors[38, 39, 30, 31, 40]. We will not be concerned with these formal aspects, but only use the concept of Floquet adiabatic or non-adiabatic dynamics mostly for interpretative purposes. In the adiabatic situation, not only do resonances' properties vary smoothly in time, as the slowly-varying field envelope modulates the adiabatic energy barrier height and width, and the energy gap at the main (one-photon) avoided crossing of the dressed potentials, but resonances (or degenerate groups of these)

are also transported smoothly, in a one-to-one manner, from one time-slice to another. Thus, if the field-molecule interaction is switched on smoothly, then an initial eigenstate of the field-free molecule will be transported adiabatically onto a single resonance and will remain in this resonance, (whose properties change slowly with time), at all subsequent times, until the end of the pulse. We will also encounter situations where the field-molecule interaction is switched on suddenly, at a time within the pulse width, when a noticeable field-intensity is already attained, defining resonance states that already differ markedly from field-free molecular eigentstates. Although the preparation of the molecule in an instantaneous Floquet wavepacket is sudden in this case, subsequent evolution of each component of this wavepacket, i.e. of Floquet resonances, may be adiabatic within the remaining part of the laser pulse. In all instances, whenever the transport of Floquet resonance states is adiabatic, their time-integrated widths are meaningful as a measure of their decay probabilities. Much of the discussion to be found in the next sections are based on this adiabatic Floquet picture. The understanding of the distinction between adiabatic and non-adiabatic Floquet dynamics is central to the interpretation of recent experimental findings in the ultra-fast pump-probe spectroscopy of dissociative ionization of dihydrogen (see section 5).

Care must be exercised to distinguish the concept of adiabatic Floquet dynamics introduced here, which refers to an adiabatic time-evolution, or to the slow variations of the Floquet basis with time, from the concept of adiabatic representation defined in the previous section, which refers to the slow variations of the electronic Hamiltonian (Floquet or not) with respect to nuclear motions, (i.e. the non-commutativity of the electronic Hamiltonian H_{el} and the nuclear kinetic energy operator T_N). Where confusion is possible and to be avoided, we shall refer to this concept of adiabaticity related to the B.O approximation as the R-adiabaticity, while adiabaticity in actual time-evolution will be termed t-adiabaticity. Non-adiabatic effects in time evolution are due to a fast variation of the (Floquet) Hamiltonian with time, causing Floquet states to change rapidly in time, to the extent that in going from one time-slice to another, a

resonance may be projected onto many new resonances as well as diffusion (continuum) states [52], and the Floquet analysis breaks down completely. We will see in section 5 how one can take advantage of such effects to image nuclear motions by an ultrafast pump-probe process.

2.5.2. Adiabaticity In Non-Floquet Representations:

An instance in which the Floquet representation breaks down, in the sense of becoming impractical, even though the field is genuinely periodic, is when the field frequency is small, as compared with the Bohr frequency of the first electronic transition at small R. The one-photon crossing is then brought to a large distance and Floquet blocks and zones are so close to each other that resonance overlaps are numerous. In such a case, it is more appropriate to discuss the dynamics in terms of the adiabatic transport of instantaneous eigenstates of the time-dependent (non-Floquet) Hamiltonian of the molecule, as this varies slowly in time[41, 10]. The diagonalization of the electronic part $H_{el}(R,t)$ of the time-dependent Hamiltonian in Eq.(2.30) and (2.36) yields potential energy curves which fluctuate in time as shown in Figure 4.1. The lower adiabatic surface is now characterized by a barrier that moves in time, both in position and in height and width. Note that these potential energy surfaces refer to an electronic representation that is both adiabatic with respect to time and with respect to nuclear motions, reflecting the two time scales, that of electronic motions, much faster, and that of the slower field oscillations that would be comparable also to the nuclear motions' time-scale. The lower adiabatic potential energy curve in Figure 4.1 supports instantaneous nuclear eigenfunctions which correspond to resonances of the shape type and, if desired, the nuclear actual wavepacket dynamics may be described and discussed in terms of these resonances. However, due to the comparable time-scales of the field oscillations and the nuclear motions, it is more useful to analyse these directly in terms of the synchonization of the time-dependent wavepacket with the moving barrier found on this lower potential energy curve. This is the framework of the analysis originally given[10] to the DDQ effect in the laser-driven dissociation of small

diatomic molecules, as reviewed in section 4.

3. Numerical Methodologies

As seen above, laser assisted and controlled photofragmentation dynamics can conceptually be viewed in two different ways. The time dependent viewpoint offers a realistic time resolved dynamical picture of the basic processes that are driven by an intense, short laser pulse. For pulses characterized by a long duration, (as compared to the time scales of the dynamics), the laser field can be considered periodic, allowing the (quasi-)complete elimination of the time variable through the Floquet formalism, giving rise to a time independent viewpoint. This formalism not only offers a useful and important interpretative tool in terms of the stationary field dressed molecular states, but also provides a more direct and accurate way to calculate the resonances involved in various laser-induced processes. We first review, in the next subsection (3.1), the computational method to actually calculate Floquet resonances in this time-independent approach as applied to the dressed H_2^+ (rotationless) molecule. The methodology used for the calculations of wavepackets in the complementary time dependent approached will then be reviewed in subsection (3.2).

3.1. Time Independent Calculations of Floquet Resonances

We present the numerical methodology for solving Eqs. (2.39), resulting from the application of the Floquet formalism to the semiclassical Hamiltonian of the molecule plus field system. For this purpose, we present Eqs. (2.39) in the generic form of a system of a finite number of closed-coupled equations

$$[T_N \mathbf{1} + \boldsymbol{\epsilon}(R))]\boldsymbol{\Psi}(R) = E\mathbf{1}\boldsymbol{\Psi}(R), \tag{3.1}$$

where, with p two-channel Floquet blocks being kept to give $N = 2p$ coupled dressed channels, $\boldsymbol{\epsilon}(R)$ is the $(N \times N)$ potential matrix appearing on the left-hand-side (lhs) of Eqs. (2.39), with elements

$$[\boldsymbol{\epsilon}]_{n,n'} = \epsilon_\kappa(R) + n\hbar\omega - \frac{E_0}{2}\mu_{ug}(R)[\delta_{n',n-1} + \delta_{n',n+1}], \quad \kappa = \begin{cases} g \leftrightarrow & n = 2k \\ u \leftrightarrow & n = 2k+1 \end{cases},$$

and **1** is the $(N \times N)$ unit matrix. The method is presented for the one-dimensional version of these coupled equations as befit the calculations of laser-induced resonances in a diatomic (rotationless) molecule perfectly aligned along the laser polarization.

Molecular channels appearing in Eqs. (2.39) belong to one of the following two classes. For a given energy E, if $E-\epsilon_{g(u)}(R)-(N-n)\hbar\omega$ goes to a positive limit $E_n = E-(N-n)\hbar\omega$ as $R \to \infty$, then the channel is open. This means that the two nuclei can separate from each other, with a relative kinetic energy $E_n = \hbar^2 k_n^2/2\mathcal{M}$, k_n being the associated wave number given by:

$$k_n = \frac{1}{\hbar}[2\mathcal{M}(E-(N-n)\hbar\omega)]^{\frac{1}{2}}, \tag{3.2}$$

If the limit is negative, then the channel is closed and the nuclei remain bounded to each other. The form of the solutions of the coupled equations, Eqs. (2.39) or Eq.(3.1) depends on the imposed boundary conditions. Consider first the case where there is at least one open channel. Scattering boundary conditions consist of imposing, for an open channel n, a combination of incoming ($\exp[-ik_nR]$) and outgoing ($\exp[+ik_nR]$) waves, while all closed channel functions are constrained to vanish asymptotically. In the case of a molecular dissociation, because of the strong interatomic repulsion prevailing at short internuclear distances, all channel functions must decay to zero as $R \longrightarrow 0$. Scattering solutions then exist with a real arbitrary energy above a certain threshold. They describe for example a situation where the nuclei approach each other with a given number of photons in the field, and then separate from each other with the same number (elastic scattering), or a different number (inelastic scattering) of photons. The scattering situation is however not the type of problem of interest in this review. When the molecule is supposed to be initially in a state belonging to a closed channel (*e. g.* a vibrational state of the ground electronic state), half-collision (or Siegert-type) boundary conditions are more appropriate. We then impose to the amplitudes associated with open channels to be asymptotically of the outgoing type only[7], while closed channel functions must vanish asymptotically as in the scattering case. This type of solution is only possible if

the (quasi-)energy is quantized and complex, of the form $E = E_R - i\Gamma/2$. Such an energy characterizes a resonance. Note that the closed or open character of a given channel as defined above must be decided using the real part of the energy. The total rate of dissociation is given by $\mathcal{K} = \Gamma/\hbar$. This can be seen from the behaviour of the associated Floquet wave function as imparted by the exponential factor containing its quasi-energy. Since a probability is calculated with the squared modulus of the wave function, this factor produces:

$$|\exp[-i\frac{Et}{\hbar}]|^2 = \exp[-\frac{\Gamma t}{\hbar}] = \exp[-\mathcal{K}t]. \tag{3.3}$$

Siegert boundary conditions also imply that the open-channel wave numbers are complex, since Eq. (3.2) is now used with a complex energy. Thus k_n can be written as

$$k_n = k_{n0} - ik_{n1}, \tag{3.4}$$

with both k_{n0} and k_{n1} positive. Since the wave function in open channel n goes asymptotically as $\exp[ik_nR]$, we have:

$$\exp[ik_nR] = \exp[ik_{n0}R]\exp[k_{n1}R]. \tag{3.5}$$

which diverges at infinity. The interpretation of this fact is the following: when measuring the outgoing flux at a distant position from the source, we are in fact interrogating the system at some time in the past. Since the source is decaying, the more distant we are from it, the more active was the source at the time of emission.

It is possible to implement explicitly Siegert boundary conditions in the determination of the multichannel wave function. An alternative approach is to transform the reaction coordinate R into a complex one $R = \rho\exp(i\vartheta)$[22]. The complex wave number k_n can also be written $\kappa\exp(-i\beta)$ with β positive. With this, the new channel function asymptotically goes to:

$$\begin{aligned} \exp[ik_nR] &= \exp[i\kappa\rho\exp(i(\vartheta-\beta))] \\ &= \exp[i\kappa\rho\cos(\vartheta-\beta)]\exp[-\kappa\rho\sin(\vartheta-\beta)]. \end{aligned} \tag{3.6}$$

If the condition $0 < (\vartheta - \beta) < \pi$ is fulfilled, the second exponential factor in the last form of $\exp[ik_n R]$ goes to zero as $\rho = |R| \longrightarrow \infty$. The channel function then behaves as that of a bound state. It is also important to note that this complex transformation of the coordinate does not affect the decreasing asymptotic behavior and the square-integrability of a bound state wavefunction. This means that any method available for bound state calculations can be used for resonance calculations. A variant of the complex rotation method consists in transforming the reaction coordinate only after some value, say R_0. The form given to the coordinate is then $R_0 + (R - R_0)\exp(i\vartheta)$. This procedure is called exterior scaling[42, 43].

For the propagation of the multichannel wave function $\mathbf{\Psi}(\mathbf{R})$, in real or complex-scaled coordinates, an efficient algorithm is furnished by the Fox-Goodwin-Numerov method[8], [44], which results from a discretization of the differential operator T_N appearing in Eqs. (2.39). Given adjacent points $R - h$, R and $R + h$ on the grid, we define an inward matrix (labelled i) and an outward matrix (labelled o) as:

$$\mathbf{P}^i(R) = \mathbf{Q}^i(R + h)[\mathbf{Q}^i(R)]^{-1}. \tag{3.7}$$

$$\mathbf{P}^o(R) = \mathbf{Q}^o(R - h)[\mathbf{Q}^o(R)]^{-1}. \tag{3.8}$$

where $\mathbf{Q}^i(\mathbf{Q}^o)$ is a matrix of independent vector solutions of the coupled-channel equations satisfying boundary conditions for inward or outward propagation respectively. The Fox-Goodwin-Numerov method actually propagates these $\mathbf{P}$ matrices on the grid. If $R - h_1$, R and $R + h_2$ are three adjacent points on the grid, either all real, or all complex or mixed, define the following (Numerov) matrices:

$$\boldsymbol{\alpha}(R) \;=\; h_2[1 + \frac{1}{12}(h_1^2 + h_1 h_2 - h_2^2)(E\mathbf{1} - \boldsymbol{\epsilon}(R))], \tag{3.9}$$

$$\boldsymbol{\beta}(R) \;=\; (h_1 + h_2)[1 - \frac{1}{12}(h_1^2 + 3h_1 h_2 + h_2^2)(E\mathbf{1} - \boldsymbol{\epsilon}(R))], \tag{3.10}$$

$$\boldsymbol{\gamma}(R) \;=\; h_1[1 + \frac{1}{12}(-h_1^2 + h_1 h_2 + h_2^2)(E\mathbf{1} - \boldsymbol{\epsilon}(R))]. \tag{3.11}$$

Then, the propagation is done with the two equations:

$$\mathbf{P}^i(R - h_1)) = [\boldsymbol{\beta}(R) - \boldsymbol{\alpha}(R + h_2)\mathbf{P}^i(R)]^{-1}\boldsymbol{\gamma}(R - h_1), \tag{3.12}$$

$$\mathbf{P}^o(R+h_2) = [\boldsymbol{\beta}(R) - \boldsymbol{\alpha}(R-h_1)\mathbf{P}^0(R)]^{-1}\boldsymbol{\gamma}(R+h_2). \tag{3.13}$$

Let R_m and $R_m + h$ be the two points chosen for the matching of the inward and outward solutions. The matching condition has the form:

$$\det|\mathbf{P}^i(R_m) - (\mathbf{P}^o(R_m+h))^{-1}| = 0. \tag{3.14}$$

The fulfillment of Eq. (3.14) generates a complex energy if the inward matrix incorporates outgoing boundary conditions (with a real coordinate), or bound state boundary conditions (with a complex rotated coordinate).

Once the complex Floquet eigenenergy has been determined from an iterative resolution of the implicit energy dependent Eq. (3.14), the multichannel wavefunction written as a column vector $\boldsymbol{\Psi}(R)$ can be calculated at the matching point because it satisfies the set of homogeneous linear equations:

$$[\mathbf{P}^i(R_m) - (\mathbf{P}^o(R_m+h))^{-1}]\boldsymbol{\Psi}(R_m) = 0, \tag{3.15}$$

The wavefunction at the other grid points can be obtained recursively from $\boldsymbol{\Psi}(R_m)$ using:

$$\begin{aligned} \boldsymbol{\Psi}(R+h) &= (\mathbf{P}^o(R+h))^{-1}\boldsymbol{\Psi}(R) \\ \boldsymbol{\Psi}(R-h) &= (\mathbf{P}^i(R-h))^{-1}\boldsymbol{\Psi}(R) \end{aligned} \tag{3.16}$$

3.2. Time Dependent Wavepacket Propagation

We now turn to the time dependent wavepacket calculations, i.e. to techniques used for solving directly the nuclear TDSE (cf. Eq. (2.11)), which for a diatomic multichannel molecule is:

$$i\hbar\frac{\partial}{\partial t}\boldsymbol{\Psi}(R,\theta,\varphi;t) = \left[\mathbf{T}_R + \mathbf{T}_{\theta,\varphi} + \tilde{\mathbf{W}}(R,\theta;t)\right]\boldsymbol{\Psi}(R,\theta,\varphi;t), \tag{3.17}$$

where R,θ,φ are the spherical coordinates of the internuclear vector $\mathbf{R}$ in the laboratory frame. The kinetic energy operators in Eq. (3.17) are given by:

$$\mathbf{T}_R = -\frac{\hbar^2}{2\mathcal{M}}\frac{\partial^2}{\partial R^2}, \tag{3.18}$$

$$\mathbf{T}_{\theta,\varphi} = -\frac{\hbar^2}{2\mathcal{M}R^2}\left\{\frac{1}{\sin\theta}\frac{\partial}{\partial\theta}(\sin\theta\frac{\partial}{\partial\theta}) + \frac{1}{\sin^2\theta}\frac{\partial^2}{\partial\varphi^2}\right\}. \tag{3.19}$$

The potential energy part $\tilde{\mathbf{W}}(R,\theta;t)$ is as defined in Eq. (2.10) for a general N-channel system. We will consider the specific case of a two-channel system, with the two coupled electronic states designated by g and u.

Eq. (3.17) is typically solved by writing

$$\begin{aligned}\mathbf{\Psi}(R,\theta,\varphi;t+\delta t) &= \mathbf{U}(\delta t)\mathbf{\Psi}(R,\theta,\varphi;t)\\ &= \exp\left[-\frac{i}{\hbar}[\mathbf{T}_R+\mathbf{T}_{\theta,\varphi}+\tilde{\mathbf{W}}(R,\theta;t)]\delta t\right]\\ &\quad\times\mathbf{\Psi}(R,\theta,\varphi;t),\end{aligned}$$

and by using a split-operator representation of the short-time propagator $U(\delta t)$:

$$\begin{aligned}U(\delta t) &= \exp\left[-\frac{i}{\hbar}[\mathbf{T}_R+\mathbf{T}_\theta+\tilde{\mathbf{W}}(t)]\delta t\right]\\ &= \exp\left[-\frac{i}{\hbar}\tilde{\mathbf{W}}\delta t/2\right]\exp\left[-\frac{i}{\hbar}\mathbf{T}_{\theta,\varphi}\delta t/2\right]\\ &\quad\times\exp\left[-\frac{i}{\hbar}\mathbf{T}_R\delta t\right]\exp\left[-\frac{i}{\hbar}\mathbf{T}_{\theta,\varphi}\delta t/2\right]\\ &\quad\times\exp\left[-\frac{i}{\hbar}\tilde{\mathbf{W}}\delta t/2\right]+O(\delta t^3).\end{aligned}$$

All propagators appearing on the right-hand-side of Eq. (3.20) are treated using the Feit-Fleck technique [23], except the one involving $\mathbf{T}_{\theta,\varphi}$, which is approximated by Cayley's formula [45]:

$$\begin{aligned}exp[-\frac{i}{\hbar}\mathbf{T}_{\theta,\varphi}\delta t/2] &= [1+(\frac{i}{\hbar})\mathbf{T}_{\theta,\varphi}\delta t/4]^{-1}\\ &\quad\times[1-(\frac{i}{\hbar})\mathbf{T}_{\theta,\varphi}\delta t/4]\\ &\quad+O(\delta t^3),\end{aligned}$$

which maintains unitarity ($\mathbf{T}_{\theta,\varphi}$ being self-adjoint) and is further implemented in a way that avoids matrix inversion.

The exponential operator containing the potential energy is straightforwardly evaluated in the coordinate representation. A prediagonalization of the instantaneous multichannel potential matrix $\tilde{\mathbf{W}}(R,\theta;t)$ is needed and naturally brings one to the (both $t-$ and $R-$) adiabatic representation described in the previous section. Fourier-transform methodology [23, 46] and, for the angular variables, a method employing either spherical harmonics basis-sets

expansions[47] or grid techniques[45] are then used to represent the exponential operators involving the radial and angular kinetic energies in Eq. (3.20). In particular, the last reference gave a significantly improved grid approach with an implementation of the above unitary Cayley scheme for $T_{\theta,\varphi}$, combined with a split operator technique using a cosine Fourier transform, resulting in a recursion formula. Apart from avoiding the numerical instabilities associated with the division by $\sin\theta$ in this angular kinetic energy term, the major advantage of this approach is the absence of matrix element evaluations and multiplications, the computational task being basically fast Fourier transforms.

Until very recently the calculations of dissociation fragments' kinetic energy spectra involved wavepacket propagations over very large grids, during the total pulse duration. A much restricted grid may be used if the wavepackets are splitted into an internal and an asymptotic part[48]:

$$\Psi_j(R,\theta;t_i) = \Psi_j^I(R,\theta;t_i) + \Psi_j^A(R,\theta;t_i) \quad (j=1,2) \tag{3.20}$$

(I for inner and A for asymptotic). The inner part is calculated by the numerical procedure described above using the restricted grid. As for the asymptotic part, the angular kinetic energy operator $T_{\theta,\varphi}$ can be omitted thanks to the R^{-2} factor it contains which tends to zero as R goes to infinity. The asymptotic region, which is the support of Ψ_j^A, is also where the field-free potential energy curves become degenerate and are flat, while the transition dipole moment between the two charge-resonant states goes as $\mu(R > R_S) \to \frac{1}{2}eR$. Because of these asymptotic behaviours of the potential matrix, the asymptotic two-state electronic system can be decoupled by an appropriate time-independent unitary transformation. The resulting decoupled equations describing field-driven nuclear motions in the asymptotic region are formally analog to the ones describing the motion of a free electron in an electric field, and admit Volkov-type analytical solutions[18]. This implies that, after Fourier transforming, the asymptotic wavepackets Ψ_j^A can be propagated analytically, avoiding the use of an extended grid, even during the field interaction[24, 49]

A much more detailed account for the split operator method and the accompa-

gnying asymptotic analysis is given in [4].

4. Processes and Mechanisms for Molecular Fragmentations in IR and UV-Vis Frequency Regimes

4.1. General Ideas

Many effects and non-linear processes induced by a laser field have been uncovered through the study of the simplest molecular system, the one-electron homonuclear diatomic H_2^+ molecule. The scope of these findings is larger though, as manifestations of these effects may be found in more complex molecules, including polyatomic systems.

The nature of these effects, the concepts required for their understanding depend on the spectral range to which the frequency of the laser field belongs. Nowadays, modern laser technology gives access to a wide range of frequencies, from Infra-Red (IR), to Visible (Vis), up to Ultra-Violet (UV) domains. Achievable peak intensities (up to tens of TW/cm^2) correspond to forces of the same order or even larger than those of the Coulomb forces that ensured the cohesion of stable molecular structures. Fields of such intensity can induce effects that are basically of two types: multiphoton effects, i.e. molecular excitations accompanying the absorptions and/or emissions of a finite number of photons, and profound modifications of molecular internal force fields. These effects have different consequences in terms of underlying mechanisms that can be exploited in control problems, for exemple, depending on the frequency domain which is adressed.

In the *UV-Vis regime* (wavelengths within 750nm to 40nm), the photon energy (a few electron-volts) is resonant with electronic transitions at some particular molecular geometry. Typically a single photon brings enough energy for the dissociation to occur, but due to the high intensity of the field, the molecule continues to absorb photons above its dissociation threshold (multiphoton ATD mechanism). The subsequent dynamics leads to fragmentation into different channels characterized by different kinetic energies associated with the absorp-

tions of different numbers of photons. As the photon frequency (larger than 5×10^{14} Hz) is high as compared to that of molecular internal motions (vibration or rotation), the molecule feels a time-averaged strong radiative field that modifies its field-free Coulomb force field. These modifications are well captured by the dressed molecule picture associated with the Floquet representation. They give rise to the softenings of some chemical bonds (barrier suppression,BS mechanism), while others are hardened (confinement or vibrational trapping, VT mechanism). New scenarios for the control of molecular reactivity can be designed by exploiting the interplay between these antagonistic mechanisms.

In the *IR regime* (wavelengths within 750nm to 0.1cm), the photon energy (less than one electron-volt) is typically resonant with nuclear vibrational motions. A single photon is not energetic enough to induce electronic excitation and/or dissociation. These processes are highly multiphotonic, requiring the accumulation of the energy of a large number of individual photons. In contrast with the UV-Vis regime, the IR laser frequency (10^{14} Hz) being comparable to internal vibrational frequencies, the molecule follows, in a time-resolved manner, the oscillations of the electromagnetic field. When properly synchronized with a vibrational mode, the laser can be used as a tool for controlling dissociation through new bond-softening or stabilization mechanisms that are proper to the IR frequency regime. Finally, it is worthwhile to note that IR laser frequencies remain high with respect to rotational motions. This gives the possibility of controlling the angular distributions of laser-driven molecules through time-averaged pendular states which govern alignment dynamics.

4.2. A Simple Model System

The general ideas outlined above are best illustrated with the exemple of electronic excitations and concomitant large-amplitude nuclear motions in the molecular ion H_2^+ under a UV-Vis and IR laser pulse. The two-channel model introduced in section 2.4, which will be recalled briefly below, is of widespread use for its ability to capture in its simplicity the essence of strong field molecular dynamics. Furthermore, the discussion can be conducted by first considering a

one-dimensional model ($\theta = 0$) representing a strictly aligned (i.e. rotationless) molecule. We thus solve the nuclear TDSE to generate wavepackets moving on the Born-Oppenheimer potential energy curves associated with two electronic states labeled g (ground, $^2\Sigma_{\rm g}^+$) and u (excited, $^2\Sigma_{\rm u}^+$),

$$i\hbar\frac{\partial}{\partial t}\begin{bmatrix}\psi_{\rm g}(R,t)\\ \psi_{\rm u}(R,t)\end{bmatrix} = \hat{H}\begin{bmatrix}\psi_{\rm g}(R,t)\\ \psi_{\rm u}(R,t)\end{bmatrix}. \tag{4.1}$$

where the Hamiltonian $\hat{H}$ is as given in Eq. (3.17) and involves a two-by-two potential operator matrix which depend on the internuclear distance R and is given by.

$$\hat{W}(R,t) = \begin{pmatrix}\epsilon_{\rm g}(R) & -E_0 f(t)\mu(R)\cos\omega t\\ -E_0 f(t)\mu(R)\cos\omega t & \epsilon_{\rm u}(R)\end{pmatrix}, \tag{4.2}$$

where $E_0, f(t)$ and ω are respectively the maximum amplitude, temporal pulse shape and carrier-wave frequency of a field explicitely taken as:

$$E(t) = E_0 f(t)\cos(\omega t + \delta). \tag{4.3}$$

The molecular dipole moment μ, which is the transition dipole between states g and u, does not contain any permanent part μ_0 for this homonuclear ion and is parallel to $\mathbf{R}$. The polarizability $\boldsymbol{\alpha}$ is not explicitely introduced as, for the intensity range we are referring to, the model can be, within good approximation, strictly limited to the lowest two BO states.

Using the wavepacket propagation methodology outlined in section 3.2, the wavepacket components $\psi_{\rm g,u}$ are generated at a given time t, from some initial state defined at $t = 0$, which will be specified later. Various observables can be calculated from the wavepackets at the current time, among which the total instantaneous probabilities for the ion to remain in bound vibrational states of the ground electronic state, *i. e.*,

$$P_{\rm bound}(t) = \sum_v \left|\langle v|\psi_{\rm g}(t)\rangle\right|^2. \tag{4.4}$$

The dissociation probability is then simply given by

$$P_{\rm diss}(t) = 1 - P_{\rm bound}(t). \tag{4.5}$$

Another observable of interest is the final probability distribution for fragments specified by their momentum k and, in two-dimensional calculations that include rotational motions, angular position θ:

$$\mathcal{P}(k) = \sum_{n=\mathrm{g,u}} \left| \tilde{\psi}_n^{\mathrm{A}}(k; t \to \infty) \right|^2, \tag{4.6}$$

where $\tilde{\psi}_{\mathrm{g,u}}^{\mathrm{A}}$ represents the Fourier transform of the asymptotic-region wavepacket components of the g and u channels respectively.

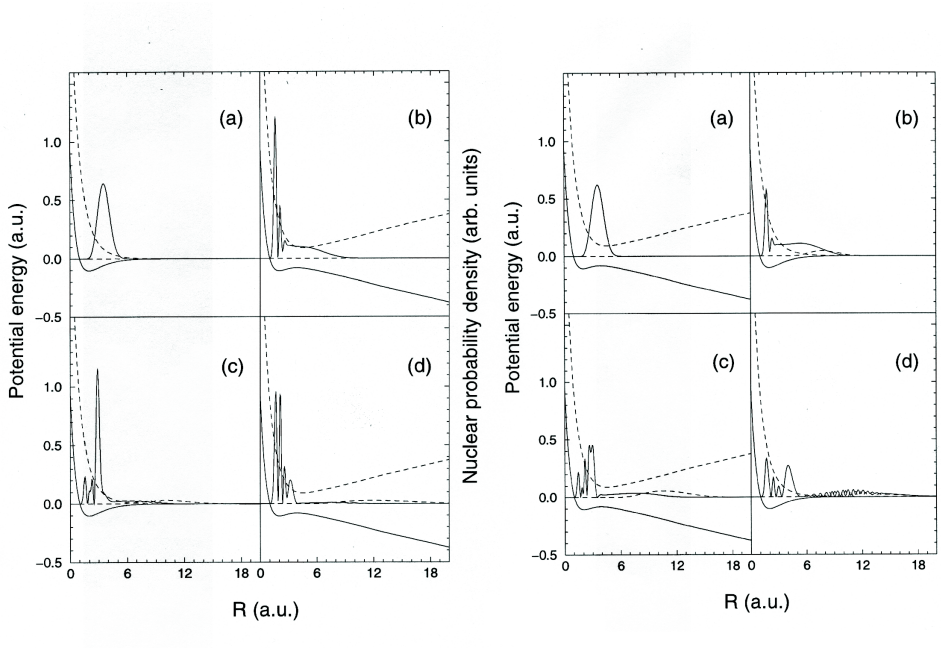

Figure 4.1: Nuclear probability distributions associated with the wavepacket supported by the adiabatic channels $W_{\pm}(R,t)$ formed under a $\omega = 943.3$ cm^{-1}, $I = 5 \times 10^{13}$ W/cm^2 laser pulse with $\delta = 0$ on the left panel and $\delta = \pi/2$ on the right panel. The wavepackets are taken at four times within the first optical cycle: (a) $t = 1/4T$; (b) $t = 1/2T$; (c) $t = 3/4T$; (d) $t = T$.

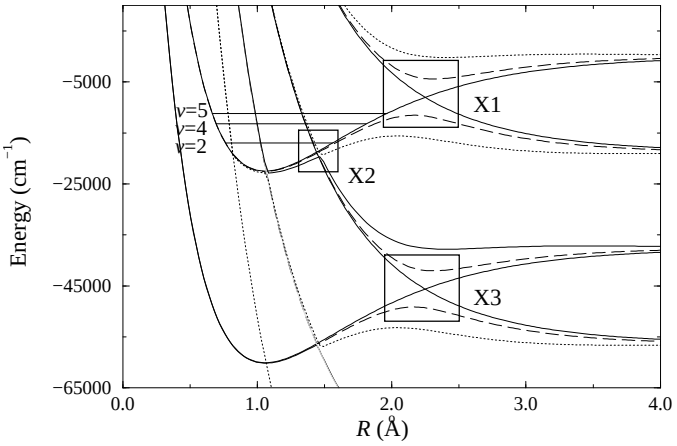

Figure 4.2: Field-dressed potential energy curves of H_2^+ (λ = 532 nm), in the diabatic (solid lines) and adiabatic (broken lines for $I = 10^{13}$ W/cm^2 and dotted lines for $I = 5 \times 10^{13}$ W/cm^2) frames. Curve-crossing regions are outlined by rectangular boxes X1, X2, and X3. The energies of the $v = 2, 4, 5$ vibrational levels are indicated by thin horizontal lines.

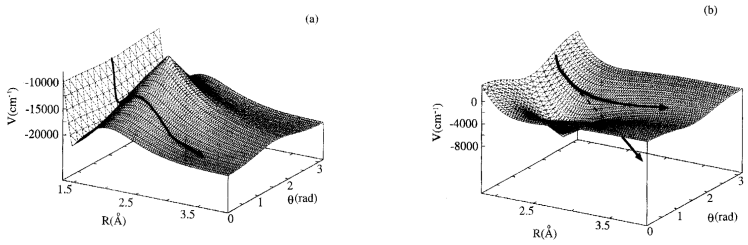

Figure 4.3: Three-dimensional graphs of adiabatic surfaces for $I = 10^{13}$ W/cm^2 in the region of the X1 (a) or X3 (b) avoided crossings. The arrows give an illustration of the minimum energy pathway on each surface.

4.3. Multiphoton Dissociation in the IR Regime

In the IR regime, the field amplitude varies typically over the same time scale as molecular vibrational motions so that a synchronization between the

nuclear motion and the laser oscillations is possible[10, 11] . This requires the definition of a time t_0 (or a related phase δ) when the field amplitude first reaches its maximum after the promotion of the initial wavepacket onto the excited electronic state,

$$\cos\left[\omega\left(t-t_0\right)\right]=\cos\left(\omega t+\delta\right). \tag{4.7}$$

For $t_0 = \delta = 0$, the initial wavepacket is considered to be prepared instantaneously at maximum intensity. In contrast, if t_0 is set equal to $T/4$ ($T = 2\pi/\omega$), corresponding to $\delta = \pi/2$, the initial state preparation occurs at the start of an optical cycle, *i. e.*, at zero field intensity. The two situations result into completely different dynamics, the former leading to dissociation quenching, while the latter is monitored by a barrier suppression mechanism. This distinction can best be understood by viewing the dynamics as taking place on the time dependent adiabatic potential surfaces $W_{\pm}(R,t)$ which arise from diagonalizing the potential energy operator of Eq. (4.2).

Figure (4.1) illustrates the dynamics of $W_{\pm}$ and of the associated nuclear probability distributions. For $\delta = 0$ the field is at its peak intensity at $t = 0$, when the initial wavepacket is prepared on the inner repulsive edge of the attractive potential W_- (close to $\epsilon_{\rm g}$ in this region). Only its tail penetrates the gap region ($R \sim 4$ a.u.) which, at that time, is widely open between W_+ and W_-. At $t = T/4$, the wavepacket components reach the gap region with a gap now closed due to the vanishing field amplitude, preventing thus any escape towards the asymptotic region. At $t = T/2$, the wavepacket is reflected back towards the inner region and the gap is open again but without any consequence with respect to an eventual escape. During the next half cycle the wavepacket motion follows the same pattern and all this leads to a stabilization of the system with respect to dissociation, which is seen to be a consequence of the bound vibrational motion being perfectly synchronized with the opening and closing of the potential gap. This is the dynamical quenching mechanism (DDQ). A completely different wavepacket motion is associated with the case $\delta = \pi/2$. Every time the wavepacket reaches the right end of the binding potential $\epsilon_{\rm g}$,

the gap is open and permits the escape of an important part of the wavepacket towards the asymptotic dissociative limit. This is the barrier lowering (and/or suppression) mechanism.

It is worthwhile to note that the field-molecule synchronization can be achieved by tuning the laser frequency and adjusting its intensity. This means that a quantitative knowledge of δ is not necessary. In particular, a two-pulse (UV + IR) scheme can be proposed with a given time delay. If an intense ultrashort UV pulse is turned on at a definite time t_0 after the onset of the long IR pulse, it will instantaneously prepares well-aligned H_2^+ ions from H_2 in its ground state. A variation of the frequency of the IR laser pulse would then allow the desired synchronization to occur[12].

Full 2D calculations (including rotations) have shown that molecular alignment is not among the necessary conditions for DDQ to be sharply observed[12]. In the case where the molecule is allowed to rotate during its interaction with the field, the efficiency of DDQ is only slightly affected. A control can thus be exerted on the system by adequately combining the laser intensity (which controls the position, the width, and the spatial spread of the gap) and frequency (which controls the gap opening and closing motions' period).

4.4. ATD Dynamics in the UV-Vis Regime

In the UV-Vis regime, the field oscillations are so fast as compared to nuclear motion that the molecular system only feels time-averaged radiatively-dressed adiabatic potentials. A transparent multiphoton interpretation to be made for the two non-linear mechanisms affecting the chemical bond (which are the analogs of the barrier suppression and DDQ of the IR regime) results from the Floquet expansion and time averaging of the molecule-plus-field Hamiltonian, valid for pulses long enough to lead to near periodic lasers. The relatively large photon energy of a UV-Vis field not only matches the electronic transition of the molecule in a modestly elongated configuration but also separates well the Floquet blocks $[(g,n);(u,n+1)$ with varying $n]$ from each other. Only a few Floquet blocks is actually needed (for a given intensity) for a converged calculation

on the network of field-dressed diabatic potentials ($\epsilon_l + n\hbar\omega$) exhibiting one-, three-photon curve crossings at short internuclear distances. This is to be contrasted with the case of an IR excitation for which the Floquet picture is rather inappropriate, as one-photon crossings occur at large distances, close to the dissociative limit, and a multitude of high-order crossings are densely produced in the inner region of the molecular potentials. Figure (4.2) shows the field-dressed potential energy curves involved in the two main Floquet blocks in the diabatic and adiabatic representations, for a typical UV-Vis filed at $\lambda = 532$ nm. Recall that the (R-)adiabatic representation, featuring avoided curve crossings, results from the diagonalization of the radiative interaction at fixed molecule-field orientations ($\theta = 0$ or π, which maximizes the couplings) and varying R. Two strong field intensities are considered, namely 10^{13} W/cm^2 and 5×10^{13} W/cm^2, at a wavelength of 532 nm, corresponding to experimental conditions[50]. The curve crossing regions upon which the interpretation of the dynamics rests are indicated by rectangular boxes: X1 and X3 correspond to one-photon crossings, between the dressed states $|g, n >$ and $|u, n-1 >$, and between $|g, n-2 >$ and $|u, n-3 >$, respectively, while X2 arises from the three-photon crossing between the ground and the two-photon channels, and X3 between $|g, n >$ and $|u, n-3 >$. Three initial vibrational states v are also shown at the level of the X1 box, with energies above ($v = 5$) or below ($v = 2$) the laser-induced barrier for both intensities or in the energy gap between the lower and upper adiabatic channel ($v = 4$).

Looking more closely at box X1, it is seen that the lowering of the laser-induced barrier at $I = 5 \times 10^{13}$ W/cm^2 is such that H_2^+ in a vibrational state $v \geq 4$ will dissociate almost exclusively by tunneling through the one-photon Bond Softening (BS) channel and leads to low energy photons. This mechanism has been abundantly discussed in the literature and experimentally verified[3, 50, 51, 53, 54]. The counterpart of BS is the Vibrational Trapping (VT) mechanisms the upper adiabatic channel may accommodate long-lived resonances[55, 56]. In particular, a very narrow resonance (of zero width, in a semiclassical estimate) may arise when a diabatic dressed vibrational level,

defined on the lower diabatic dressed PES ($\epsilon_l + n\hbar\omega$), is close to a level created on the upper adiabatic PES[57]. Such coincidences may be obtained at will by just properly adjusting the laser wavelength (*i.e.* the relative energy positioning of the potentials) and intensity (*i.e.* the strength of the coupling)[55, 58]. When the molecule is properly prepared (by an adiabatic excitation, using a pulse with a sufficiently long rise time) in such a resonance state, good stabilization is expected[56]. Early works even proposed an isotope separation scenario in a H_2^+/D_2^+ mixture based on this vibrational trapping mechanism[55]. The scheme relies on the great sensitivity of the aforementioned diabatic-adiabatic level coincidences with respect to the laser and molecular characteristics. A coincidence that has been obtained for a molecule-plus-field system would no longer hold when one proceeds to an isotopic substitution, because of mass-related energy shifts. A detailed account of this mechanism will be given in section 6. It is to be emphasized that the two stabilization mechanisms in consideration, here and in the previous subsection, have completely different origins: The DDQ effect in the IR regime is based on a dynamical effect whereas the VT effect in the UV-Vis regime is a pure stationary process. These basic mechanisms not only help in controlling molecular dissociation and understanding fragments kinetic energy distributions, but they can also be referred to for the interpretation of angular distributions of fragments in the strong-field photodissociation process.

To this end, it would be necessary to relax the restriction to a one-dimensional model and allow for rotational motion described by the angles θ and φ. In fact, for a linearly polarized field, the time-dependent Hamiltonian has axial symmetry and only the angular variable θ needs be considered explicitly. Figure (4.3) presents 3D graphs of the (two-dimensional) adiabatic PESs in the region of the X1 and X3 avoided crossings. Imagine an initial wavepacket prepared on the short range repulsive limit of the surface pictured in Fig. (4.3(a)). It will be propagated towards the X1 region where the adiabatic potential barrier height is modulated by the angle-dependent laser-molecule coupling, *i. e.*, to $\mu E_0 \cos\theta$. For a given field strength, this lowering is more pronounced for $\cos\theta \sim 1$ ($\theta \sim 0$ or π). For $\cos\theta \sim 0$ ($\theta \sim \pi/2$) the higher potential barrier is hardly pene-

trable. Under the effect of the torque exerted by the laser on the molecule, the wavepacket skirts around the potential barrier and follows the minimum energy pathway of the dissociative valley (that is for directions close to $\theta = 0$ or π) resulting in aligned fragments when the BS mechanism is operative[49]. Figure (4.3(b)) represents, in the X3 region, the adiabatic surface leading to dissociation corresponding to the net absorption of two photons. To reach this surface, a large portion of the initial wavepacket has to undergo a non-adiabatic transition at X2. The non-adiabatic coupling responsible for the dissociation is sharply peaked around the avoided crossing position X2 with a strength that is much larger for $\theta \approx \pi/2$ (there is no coupling at $\theta = \pi/2$) than for $\theta = 0$ or π[49]. The wavepacket prepared on this surface presents an angular distribution more pronounced around $\theta \sim \pi/2$. Subsequent dissociation dynamics on this surface also favors the $\theta \sim \pi/2$ direction as this corresponds to a potential valley. Finally, less aligned fragments are expected when non-adiabatic transitions are responsible for the dissociation of an initially trapped configuration.

We continue in the next two Sections with two separate applications of the basic mechanisms discussed here: (i) A thorough interpretation of a recent pump-probe study of the dissociative ionization of H_2 and (ii) A study of control scenarios for molecular cooling and vibrational population transfer using Zero-Width Resonances (ZWRs) and the related concept of Exceptional Points (EPs).

5. XUV+IR Pump-Probe Spectroscopy of Molecular Dissociative Ionization

5.1. Introduction

With recent advances in laser technology, in particular with the generation of attosecond laser pulses as a spin-off of research on High-Harmonic generation (HHG), the real-time imaging of ultrafast molecular phenomena has become accessible. Just as femtosecond laser pulses led to the development of transition state spectroscopy and femtosecond chemistry [59], the advent of attosecond pulses [60] has given rise to endeavours where it is the even faster electronic

motion that is probed in a time-resolved manner [61]. An important concern in these experiments is the question as to which extent the structure and dynamics of the molecule under investigation are influenced by the presence of the intense infrared (IR) laser field that drives the high-harmonic generation process [62]. In the previous section, we have evoked the use of an ultrafast UV or XUV (pump) pulse to trigger the ionization of a molecule such as H_2 within the width of a longer IR (probe) pulse, which would cause the dissociation, or the vibrational trapping, of the molecular ion depending on the delay between the two pulses and the frequency of the IR pulse, in a possible direct experimental study of the DDQ effects. A similar set of experiments has been performed recently, but with the probe pulse being in the near IR rather ($\lambda = 750\ nm$) for which the Floquet dressed molecule picture still applies, so that instead of monitoring the DDQ type control, these experiments rather map out the degree of adiabaticity of the Floquet dynamics under the probe near-IR pulse (henceforth refered to as the IR pulse). We now review these experimental results and the accompanying theoretical interpretations[25],[26], and discuss the roles of different type of resonances associated with the Floquet representation in the very rich dynamics reflected in these results.

5.2. Experimental context

Two experiments were performed using an extreme ultra-violet (XUV) attosecond pump pulse, ($\hbar\omega \simeq 35.eV$), which creates an initial vibrational wave packet on the $H_2^+, 140\ as$ FWHM ($1s\sigma_g^+$) potential by means of a single photon ionization of H_2. This (XUV) pump pulse thus serves to accurately define the time of ionization of the molecule, with respect to which subsequent dissociation of the H_2^+ ion is clocked, with the initial H_2^+ geometry reflecting that of the neutral ground state. The two experiments differ primarily in terms of the properties of the near IR field ($\lambda = 750\ nm$) that is used. In one experiment, henceforth called experiment A, the IR pulse is significantly shorter than the H_2^+ vibrational period ($7\ fs$ Full-Width at Half Maximum [FWHM]). In contrast, in experiment B, the duration of the IR laser pulse ($35\ fs$ FWHM) is comparable

to (slightly longer) than the H_2^+ vibrational period, meaning that the IR field is present during the propagation of the wave packet before dissociation, which, depending on the XUV-IR delay, τ, may or may not include the time at which the ionization by the XUV took place. In both cases, this delay is defined as the time separating the crest of the IR pulse from the peak of the XUV pulse, so that $\tau > 0$ denotes the situation where the XUV pulse precedes the IR pulse[4].

Figure (5.1) shows a comparison of how the H^+ fragment kinetic energy (KE) distributions measured in experiments A and B varies as a function of the delay τ. In experiment A, the yield of fragments with energies below 1.2 eV exhibits a beating pattern with a main period of about 27 fs. A closer analysis of this pattern, visible even at the most coarse-grained level, as obtained by integrating the experimental H^+ KE distribution over the energy range of 0-1.2 eV, as shown in Figure (5.2), [panel (a) of this figure shows this integrated signal as a function of τ, while panel (b) shows its Fourier transform], reveals that the oscillatory signal arises from the beating of a number of frequencies that are basically the Bohr frequencies between adjacent field-free vibrational levels around $v = 9$. This experiment A thus seems to be imaging just the vibrational content of the initial wavepacket. The results for experiment B, where the IR pulse duration is somewhat longer than the vibrational period of the H_2^+ molecule, are radically different. In this case, the proton kinetic energy distribution evolves smoothly as a function of τ. The most important feature in this smooth τ-dependence is the red shift of the center of gravity of the spectrum as τ increases past the interval denoting XUV-IR pulse overlap, to stabilize at a low level of $.25\ eV$, for all positive values of τ denoting the situation where the IR pulse clearly follows the XUV pulse ($\tau > 20\ fs$). No oscillatory pattern is seen in the experimental results for this case.

[4]Note that the IR pulse generated high harmonics that were used to make the attosecond XUV pulses. As a consequence, in the case of the 35 fs IR field, one has a train of a finite number of attosecond pulses serving as the XUV pump, rather than a single one. We will ignore this distinction in the following.

5.3. Theoretical Simulations

In order to simulate the experimental results, concentrating on the dissociation of H_2^+ after its preparation by the XUV pulse, the one-dimensional two-channel model described in previous sections was used. We thus consider the H_2 parent molecule, originally in its ground vibrational and electronic state, to be ionized by the XUV pulse at time t = 0 and that the ionization is merely a Franck-Condon (FC) vertical promotion of the $v = 0$ vibrational state of the parent molecule onto the ground electronic state $|1s\sigma_g^+\rangle$ of the molecular ion. Subsequent nuclear wavepacket motions then develop on the two electronic manifolds of the molecular ion H_2^+, the ground state $|1s\sigma_g^+\rangle$ and the first excited electronic state $|2p\sigma_u^+\rangle$. The molecule is assumed to be aligned along the laser polarization. This is justified not only by our wish to concentrate on the essential feature of the dynamics, but also by the fact that experimentally, the angle-resolved H^+ detection allows one to selectively observe fragments along the polarization axis, and it was found that none of the observations reported, and summarized in Figure (5.1) depends very strongly on the ejection angle of the H^+ fragment with respect to the polarization axis. As for the results shown in the preceding section, the wavepacket propagation procedure described in section 3.2, but restricted to just the radial dimension, is used, and the proton kinetic spectra is extracted from the relative momentum k distribution defined in Eq.(4.6). The calculations are repeated for an extensive range of values of τ, (more details on the calculations can be found in [26]), and produced the results shown in Figure (5.3), which displays the theoretical proton KE distributions as a function of τ for the same IR pulse durations as in experiments A and B, at intensities of $1 \times 10^{13}\ W/cm^2$ and $3 \times 10^{13}\ W/cm^2$ respectively, which corresponds to the estimated peak intensities in the experiments. The calculations give spectra with much better detailed structures than the experiment. However the main observations of the experimental Figure (5.1), as detailed above, are well brought out: In the case of the shorter IR pulse (experiment A), the same beating pattern, though much better resolved, is found when the KE spectrum is viewed as a function of the delay τ. Again this is in marked contrast with the

results of the calculations for the longer IR pulse, which give a much smoother variation of the various features in the proton KE spectrum as a function of τ, although the lowest energy band does show a residual beating pattern. Of note again is the global red shift of the whole spectrum as τ increases from zero to ca. 20 fs.

5.4. Adiabatic vs. Non-adiabatic Floquet Resonance Dynamics

In the condition of experiment A, as long as τ is larger than the width of the IR pulse so that no pulse overlap is possible and the IR pulse clearly follows the XUV pulse, the coherent superposition of vibrational states of H_2^+ prepared by this pump pulse (the Franck-Condon wavapacket) evolves under essentially field-free conditions, oscillating back and forth and spreading out on the $1s\sigma_g^+$ potential, before encountering the IR pulse. The shortness of the IR pulse evokes a limiting situation (a "sudden" dissociation limit), where the laser-molecule interaction merely opens, for a very brief instant, (around the peak of the already short IR probe pulse), a "gate" to dissociation at some internuclear distance. The dissociation yield at any (half-collision) energy, measured essentially by the squared moduli of the wavepackets evaluated at this gate, thus depends on a synchronization between the wavepacket and the opening of this gate at the maximum of the IR field. This synchronization is a result of the coherence between the various vibrational components of the initial wavepacket and the dissociation yield necessarily reflects that coherence in this case. The dominant, coarse-grained behaviour of the KE spectrum as a function of τ, the beating pattern reflecting the coherence of the initial vibrational wavepacket, i.e. field-free vibrational states, carries no or little specific information on laser-induced resonances, as the adiabatic Floquet picture breaks down completely for such a short IR pulse. The wavepacket/gap synchronization evoked above is rather reminiscent of the DDQ effect, denoting a dynamical effect rather than a static, structural one.

Turning now to the case the H_2^+ vibrational wavepackets interact with a longer, 35 fs FWHM, IR pulse (experiment B), a behaviour denoting a somewhat

more adiabatic Floquet dynamics is expected, and little or no dependence of the KE spectrum on the time delay τ should be found as long as the XUV pulse precedes the IR without overlapping. This is what is indeed observed at time delays $\tau > 20$ fs. The residual oscillatory found in the computed τ-dependent spectrum indicates that t-non-adiabatic effects are present though, and this is hardly surprising as the 35 fs IR pulse features strong modulation of this laser's intensity over a time scale that is only about ten times the period of the carrier wave. For $\tau < 20\ fs$, the fragment KE spectrum is strongly delay-dependent, curving up smoothly as τ decreases to reach energy values similar to those encountered in the experiment A near zero delay.

This dependence of the H^+ KE on the XUV-IR delay in this case of the longer, 35 fs FWHM, IR pulse can be understood in terms of the adiabaticity of the Floquet dynamics underlying the dissociation processes, and the way that the IR intensity affects both the preparation and the propagation of the Floquet components of the wavepackets. More precisely, the IR probe pulse projects the various vibrational components of the wave packet onto Floquet resonances, whose widths vary with the intensity of the IR pulse. We recall that these resonances are of two types: Shape resonances supported by the lower adiabatic potential defined at the one-photon crossing between the dressed (g, n), (u, n') channels and leading to efficient dissociation through the BS mechanism, or Feshbach resonances, vibrationaly trapped in the upper adiabatic potential well.

When the IR pulse follows the XUV pulse without overlapping (i.e. $\tau > 20fs$) individual field-free vibrational states v^+ of the ion are, at first, transported adiabatically onto corresponding Floquet resonances. Each resonance gives rise to a characteristic line in the proton KE spectrum. The magnitude of the KE is determined by the non-perturbative laser-induced modification of the dressed potential energy curves. On the way towards dissociation, the ion experiences the increasing in time of the IR pulse amplitude and therefore sees a lowering of the BS barrier. The lowest barrier height is reached at mid-pulse time (maximum of intensity), resulting in most efficient dissociation when the lowest energy shape resonance can still tunnel through before the barrier rises.

Most protons contributing to the spectrum have a KE of about 0.3 eV corresponding to the shape resonance issued from $v^+ = 8$. Higher energy shape resonances are also dissociative, but are not significantly populated by the XUV ionization step (through FC mapping of the vibrationless ground state of H_2).

This situation is to be contrasted with the case where the IR and XUV pulses are overlapping ($\tau < 10fs$), i.e the H_2^+ ion is prepared at a moment when the IR field already has an appreciable intensity, and Floquet resonances defined by that field already differ markedly from field-free vibrational states. In this case, it can be said that the vibrational states of the ion are shaken up by this sudden intense IR excitation and are all instantly projected onto a superposition of shape and Feshbach resonances and these now appear in the wavepacket with weighting coefficients that may differ noticeably from those characterizing the FC wavepacket in terms of field-free states. In particular, higher energy resonances may temporarily be populated and take an important part in the dissociation step. Afterwards, as shown in Figure (5.4b), the ion experiences the falling edge of the IR pulse with a rising BS barrier which quenches the dissociation of low energy shape resonances. High energy over-the-barrier shape resonances, more populated than in the previous adiabatic case, are the ones which contribute most to the dissociation. This explains the blue-shift of the protons KE distribution when τ decreases, bringing the XUV pulse closer to the maximum of the IR probe, with the increasing role played by resonances issued from $v^+ = 9, 10$ leading to a spectrum centered at about 0.5 eV.

To obtain a better, quantitative experiment versus theory agreement would require the relaxation of some of the assumptions inherent in our model. Among these approximations are a phenomenological description of the XUV ionization step[63], the neglect of rotational degrees of freedom [64] and also of the neglect of such realistic effects as laser focal volume averaging [64]. Nevertheless, the analysis just given shows how the dynamics of the two-colour dissociative ionization of H_2 under the influence of an XUV+IR pump-probe pulse sequence depends considerably on the adiabaticity of both the initial Floquet

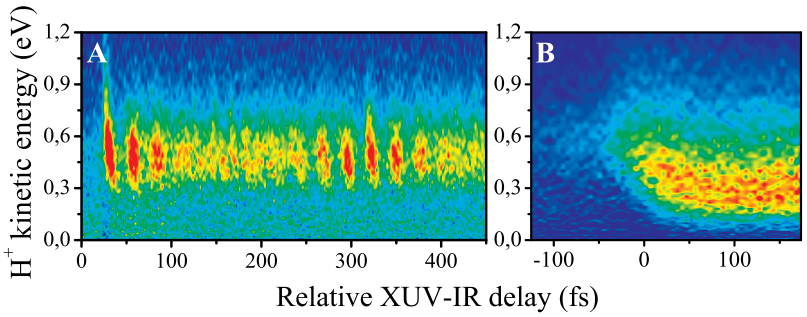

Figure 5.1: Measured time-dependent H^+ kinetic energy distributions for two-colour XUV+IR dissociative ionization of H_2, with 7 fs IR laser pulses (A) and 35 fs IR laser pulses (B).

wavepacket preparation and the Floquet states' transport under the IR pulse. The present work represents a departure from most intense field dynamics work. Ordinarily, adiabatic laser excitation regimes result in spectral observables with finely resolved peak structures that can be interpreted in terms of isolated, non-overlapping resonances [65], while a sudden and strong laser excitation normally induces overlapping of large width resonances, erasing specific dynamical information (leading to structureless and less informative spectral data). Rather, the two experimental situations described here and their interpretations illustrate how the richness of the structural determination of molecules, their imaging and possible control in these situations rest on the sudden (non-adiabatic) or gradual (adiabatic) character of the strong IR excitations.

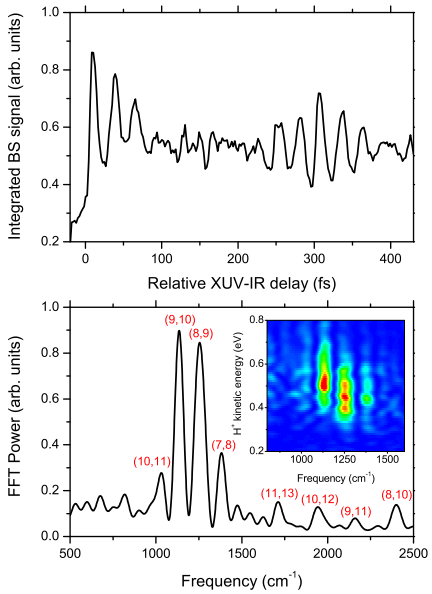

Figure 5.2: (a) Time-dependence of the H^+ fragment yield (obtained by integrating the measured KE distribution between 0 and 1.2 eV) as a function of the XUV-IR delay. The fragment yield shows oscillations resulting from the motion of the vibrational wave packet on the $1s\sigma_g^+$ potential. Clear indications of wave packet de-phasing and re-phasing are observed; (b) Fourier Transform of the measurement shown in (a), revealing the two-level beats that are responsible for the observed time-dependence. The inset shows a KE-resolved Fourier Transformation of the experimental results, and reveals a correlation between the fragment KE release and the vibrational level occupied prior to dissociation.

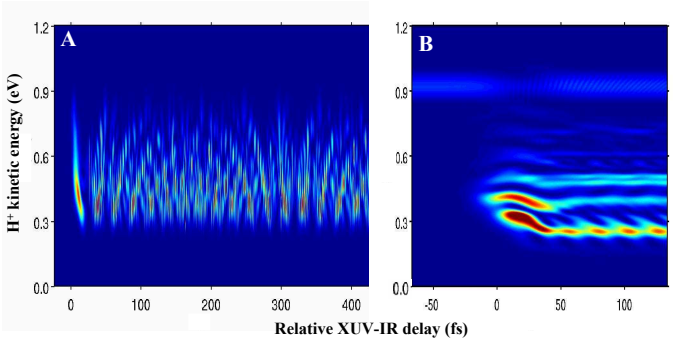

Figure 5.3: Comparison of the time-dependent kinetic energy distributions resulting from model calculations for two-colour XUV+IR dissociative ionization of H_2, making use of a 7 fs IR pulse (A) and a 35 fs IR pulse (B).

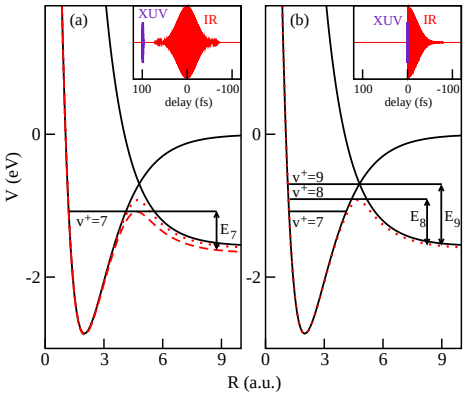

Figure 5.4: Potential energy curves of H_2^+ in a 750 nm laser-dressed diabatic representation (black solid lines). Are also indicated the lower adiabatic curves resulting from the diagonalisation of the radiative interaction for two intensities ($I = 3 \times p10^{13}$ W/cm^2 reached at mid-pulse time, in red dashed line and $I = 10^{13}$ W/cm^2 in doted red line). E_7, E_8 and E_9 represent the kinetic energies issued from $v^+ = 7$, 8 and 9 for the typical XUV-IR delays (about 100 fs (a) and 0 fs (b)).

6. Zero-Width Resonances and Exceptional Points in molecular photodissociation

6.1. Introduction

We consider again a (diatomic) molecule with a ground electronic state represented by an attractive Born-Oppenheimer potential energy curve and a first excited state represented by a repulsive potential. The H_2^+ model system considered in the preceeding sections is a typical exemple of such a system. Imagine first the molecule exposed to a continuous wave (cw) laser field. Within the Floquet formalism, the photodissociation rate can then be calculated quantum mechanically by the Fox-Goodwin-Numerov algorithm, as described in section 3.1, for a realistic $N = 2p$-channel, p-Floquet-block model, but it can also be obtained with a semiclassical approach whenever the intensity is such as to justify for a two-channel approximation. The semiclassical approach has been originally developped to treat predissociation [57] and has been useful in showing that under some particular circumstances the predissociation rate could be vanishingly small. In the semi-classical theory of predissociative systems, their occurence can be traced back to the existence of two kinds of zeroth-order states with energies which come in close coincidence. The disposition of the potential energy curves in the dressed molecule picture is similar to that of a predissociative system, and thus can give rise to Zero-Width Resonances (ZWR). It has been shown [58, 14, 6] that it is indeed possible, for a given wavelength and for a given resonance issued from a vibrational state of the field-free molecule, to find a laser intensity at which the resonance width and hence the photodissociation rate vanishes. We call such an intensity a critical intensity. The flexibility in choosing laser frequency and intensity conditions to tune predissociation-like couplings and curve crossing is at the origin of another interesting phenomenon: Resonance coalescence, *i. e.*the coincidence of the complex energies and wavefunctions of two resonances, which is attainable for specific laser wavelengths and intensities, leading to the so-called Exceptional Points (EP)[15]. Such points are present in many areas of physics, with examples in classical physics [66, 67],

as well as in quantum physics [68, 69]. We give here a review of these ideas, starting with the semiclassical expression of the condition for the appearance of a Zero-Width Resonance, the physical definition of the EP, before illustrating the two concepts and their use in vibrational control problems. We will be showing results of two types of calculations: Explicit intensity dependent resonance energies and widths are obtained by the time-independent approach detailed in section 3.1 applied to the Floquet N-channel closed-coupled equations, Eqs. (2.39) or (3.1), $N = 2, 4$ or 6, corresponding to keeping one, two or three Floquet blocks. Results of wavepacket calculations for adiabatic, long pulses will also be shown to verify predictions made based on just the resonance properties, in particular on those of ZWR and EP. These results are obtained with the time-dependent wavepacket propagation procedure detailed in section 3.2, mainly in the one-dimensional version, *i. e.*with just the radial dimension, ignoring rotational effects.

6.2. Semiclassical theory

Semiclassical theory of predissociation of a diatomic molecule [57, 70] states very clearly the conditions for the occurrence of Zero-Width Resonances. This formalism is also applicable to laser-induced resonances given the analogy between the potentials describing predissociation and those of Figure (6.1) arising from the dressing of a two-channel molecule by a field. The potentials involved in the semiclassical treatment are indicated in the right panel of Figure (6.1). For predissociation the interchannel coupling is a property of the molecule. For intense field photodissociation, the parameters controlling the couplings are those of the external field and, in principle, can be tuned at will. The semiclassical formalism provides analytic formulas for the resonance width. It predicts [57, 70] that if the energy is such that the two following conditions are simultaneously satisfied

$$\int_{R_+}^{R_0} dR\ k_+(R,E) + \int_{R_0}^{R_t} dR k_+(R,E) + \chi = (\tilde{v}_+ + \frac{1}{2})\pi \qquad (6.1)$$

and

$$\int_{R_-}^{R_0} dR\ k_-(R,E) + \int_{R_0}^{R_t} dR k_+(R,E) = (\tilde{v} + \frac{1}{2})\pi \tag{6.2}$$

with $\tilde{v}_+$ and $\tilde{v}$ some integers, then the outgoing scattering amplitude in the lower (open) adiabatic channel is zero, with the consequence that the predissociation is quenched. In Eqs.(6.1,6.2) the energy-dependent wave numbers are $k_\pm(R,E) = \hbar^{-1}[2\mathcal{M}(E - V_\pm(R)]^{1/2}$, $\mathcal{M}$ being the nuclear reduced mass. $R_\pm$ are the left turning points of the lower and upper adiabatic potentials $V_\pm(R)$, whereas R_t is the right turning point of $V_+(R)$. These conditions are nothing but Bohr-Sommerfeld quantization conditions. They mean that there is coincidence of two energy levels: $E_{\tilde{v}_+}$ supported by the upper adiabatic potential, affected by a phase correction χ, which is $-\pi/4$ in the weak coupling limit[70], and $E_{\tilde{v}}$ supported by a diabatic-like potential presenting a discontinuity and defined as follows: On the left of the diabatic crossing point R_0 this potential is the lower adiabatic potential, while beyond this point it is the upper adiabatic potential. For a weak coupling, this is practically the diabatic attractive potential. We call these two kinds of energies the "modified" diabatic and adiabatic energies respectively. The coincidence condition can then be appreciated with the expression for the resonance width Γ_v which emphazises the role of the proximity of the two kinds of energies [70]:

$$\Gamma_v = \frac{2\pi}{\hbar} \frac{e^{2\pi\nu}(e^{2\pi\nu} - 1)\omega\omega_+}{(\omega_+ + (e^{2\pi\nu} - 1)\omega)^3}(E_{\tilde{v}} - E_{\tilde{v}_+})^2, \tag{6.3}$$

where ω and ω_+ are local energy spacings of the modified diabatic and adiabatic potentials. ν is the coupling parameter, which, in a Landau-Zener type of approximation, is given in the laser induced photodissociation problem, represented by a single Floquet block, by

$$\nu = \frac{\mu^2(R_0)\mathcal{E}_0^2}{\hbar\overline{v}|\Delta F|}, \tag{6.4}$$

$\overline{v}$ and ΔF are the classical velocity and the difference of slopes of the diabatic potentials at the diabatic crossing point R_0. $\mu(R_0)$ is the electronic transition

moment at the diabatic crossing point and $\mathcal{E}_0$ the electric field amplitude of the laser field.

In the predissociation problem the coincidence can only be accidental since the potentials and the coupling cannot be modified. For a diatomic molecule submitted to an electromagnetic field, the wavelength and the intensity of the field are two external parameters which allow one to produce at will such coincidences. This explains the occurrence of Zero-Width Resonances (ZWRs) in laser induced photodissociation. Such a flexibility can also be exploited to produce the Exceptional Points (EPs) occuring in this context.

6.3. Zero-Width Resonances and coalescence at an Exceptional Point

Figure (6.2) displays the rates as a function of intensity for two resonances issued respectively from the field-free vibrational states $v = 8$ and $v = 9$, for a wavelength $\lambda = 255.255$ nm. Of note is the existence of an intensity where the rates, i.e. the imaginary part of the two resonance energies, approach each other. This signal the existence of an Exceptional Point (EP) in the laser parameter (intensity, frequency) space. The left panel is a zoom of the curves near the Exceptional Point. Similar features are found in many other areas of physics including optics, atomic physics, electron-molecule collisions, superconductors, quantum phase transitions in systems of interacting bosons, electric field oscillations in microwave cavities, to, more recently, molecular physics[27]. We note that the rate of the resonance $v = 9$ can shoot up to very high values. This has been interpreted [71] as due to the shape character of such resonances, which in zeroth order (in the channel couplings), are associated with energies marked as $E_{\tilde{v}}$ in Figure (6.1). The resonances associated with energies marked as $E_{\tilde{v^+}}$ are interpreted as having a Feshbach-like character. Their widths go asymptotically to zero, since the coupling of the upper diabatic potential with the lower one decreases as the intensity increases. The right panel of Figure (6.2) shows that the rate of level $v = 8$ reaches zero twice. This multiple occurrence of the zero-width phenomenon has been related to the possibility to produce several times a diabatic-adiabatic coincidence as the intensity increases [71]. This is

so because the adiabatic (vibrational) levels goes up faster than the diabatic ones and therefore a given adiabatic level can cross several diabatic levels as the intensity increases. It is to be noted that resonance coalescence, *i. e.*the existence of an (EP), requires an appropriate choice of both frequency and intensity, while a ZWR would show up at some critical intensity(ies), irrespective of the choice of the wavelength, for all resonances of Feshbach type. One must keep in mind that the classification into shape and Feshbach depends strongly on the wavelength.

6.4. Vibrational Purification Using ZWR

At $\lambda = 420$ nm, the resonances $v = 8$ and $v = 10$ can acquire a zero width as, with increasing intensity, they tend to merge each into some bound state of the upper adiabatic potential, actually with states given respectively by quantum numbers $\tilde{v}_+$ equal 0 and 1. In contrast, resonances 7 and 9, which are of shape type, can acquire very large widths when the intensity increases, due to the progressive lowering of the barrier of the lower adiabatic potential. Figure (6.3) shows (lower panel) how the rates of these four resonances actually vary as an function of time, considered a parameter in correspondence with the instantaneous electric field of the pulsed laser shown in the top panel. Clearly the width of resonance 8 goes through zero twice, while the laser intensity never got large enough throughout the pulse for the rate of resonance 10 to go to zero. It is interesting to compare at this point results of time-dependent wavepacket calculations starting from field-free vibrational states with $v = 7 - 9$, with those predicted by accumulating the widths of the above Floquet resonances over time, assuming a pure adiabatic transport of these resonances under the pulse shown in Figure (6.3). The observable considered here, the probability for the system to remain bound, while it adiabatically evolves as a pure Floquet resonance v (which, at zero-field, correlates with the vibrational state of the same v) under a pulse of total duration t_f is[6]:

$$P_b(v; t_f) = \exp\Big[- \int_o^{t_f} \Gamma_v(t')dt' \Big]. \tag{6.5}$$

On the other hand, in the direct time-dependent approach, the survival probability, i.e., the probability for the system to remain bound at the end of the pulse, adapting Eq.(4.4), is [6] :

$$P_{bound}(v;t_f) = \sum_{v'} p_{bound}(v,v';t_f), \tag{6.6}$$

where

$$p_{bound}(v,v';t_f) = \frac{|\langle v'|\psi_g^{(v)}(t_f)\rangle|^2}{|\langle\psi_g^{(v)}(t_f)|\psi_g^{(v)}(t_f)\rangle|^2 + |\langle\psi_u(t_f)|\psi_u(t_f)\rangle|^2}, \tag{6.7}$$

The sum is taken over all the discrete vibrational levels v' of state $|g\rangle$. $\psi_g^{(v)}(t)$ is the component of the wave packet on the g channel evolved up to time t from the field-free vibrational state $|v>$ prepared at time $t = 0$. Note that $P_{bound}(v;t_f)$ actually represents the total bound state population at any time after t_f, since no further decay is then possible, the laser being turned off at such a time. It is clear that Eq.(6.5) gives a useful approximation for the result of a full time-dependent wavepacket evolution, [Eq.(6.7)], only if the assumption of an adiabatic transport of Floquet states is valid.

Figure (6.4) gives an example of such a comparison, considering specifically the evolution of the molecule out of the $v = 7$ state, under a $\lambda = 420$ nm, $I = 0.05 \times 10^{13}$ W/cm^2, 56 fs long pulse of the same form as shown in Figure (6.3). An excellent agreement is note. In fact, this agreement holds not only for the final value of the probability for the molecule to remain bound after the pulse is over, but also for the survival probability evaluated at any time during the pulse.

Figure (6.5) further compares the results of the two types of calculations for a series of resonances at a higher peak intensity of the same pulse. Two conclusions emerge. First, the adiabatic Floquet formalism is again validated by the rather good agreement. Second, as expected, the state which is best protected against dissociation is $v = 8$, this being clearly related to the fact that only this state benefits, in this example, from a width which does vanish at least once while the pulse is on. A different way to check how the different

states react to the field is to start from a coherent combination of vibrational functions and to follow in time the evolution of this combination. The initial wave packet is taken as $|\tilde{\psi}(t=0)>=3^{-\frac{1}{2}}[|7>+|8>+|9>]$. For the pulse used for this level-by-level study, shown in Figure (6.3), upper panel, we obtain now for the probability to find the system remaining bounded at the end of the pulse, the total value of

$$P_{bound} = 0.2960. \tag{6.8}$$

with the following breakdown into 3 dominant contributions that are

$$P_{bound}(7;t_f) = |<7|\tilde{\psi}(t_f)>|^2 = 0.0021, \tag{6.9}$$

$$P_{bound}(8;t_f) = |<8|\tilde{\psi}(t_f)>|^2 = 0.2852, \tag{6.10}$$

$$P_{bound}(9;t_f) = |<9|\tilde{\psi}(t_f)>|^2 = 0.0044. \tag{6.11}$$

It is thus the resonance issued from the level $v=8$ that contributes most to the survival probability, which is not surprising as the resonance's width goes twice through a zero value during the pulse.

A ZWR may also offer an original isotope separation technique. A coincidence of the "modified" diabatic $E_{\tilde{v}}$ and adiabatic $E_{\tilde{v}_+}$ energies such as those involved in Eq.(6.3), supposedly ensured for a given molecule-plus-laser system would no longer hold when one proceeds to an isotopic substitution. The feasibility, selectivity and efficiency of an isotope separation in a mixture of D_2^+ / H_2^+ is proven in Figure (6.6) [58]. For a laser wavelength of 120nm we examined the $v=2$ resonance for both D_2^+ and H_2^+. A ZWR for D_2^+ is reached at an intensity of about 1.1×10^{13} W/cm^2. It is important to note that while the width attains a minimum (which is actually a zero) for D_2^+, it acquires a rather large value, Γ_2=600 cm^{-1} for H_2^+, (the rates of Figure (6.6) are twice the corresponding widths). We have thus shown that with a specific choice of the laser wavelength and intensity, D_2^+ dissociation may completely be suppressed, whereas for the same field H_2^+ is still strongly dissociative: This is an original isotope separation scheme by laser-induced purification of D_2^+ in a mixture of D_2^+ / H_2^+.

6.5. Vibrational transfer around an Exceptional Point

We turn now to an exploitation of the other feature of Figure (6.2). We have seen that it is possible to make a choice of laser intensity and frequency which produces a near coalescence of two resonance energies. Because of the numerical character of the exploration, it is difficult to be accurately on the Exceptional Point. However there is a property of such a point which can be checked even when its position is known with a limited accuracy: Driving adiabatically the system along a closed loop encircling an EP should produce a resonance tranfer. Starting from one of the resonances involved in the EP, the final result is that the molecule must end up in the other resonance [27, 16, 72]. We illustrate this property of an EP in Figure (6.7), with the initial state being $v = 9$. The loop in the parameter plane is defined by the two relations

$$\lambda = 255.25\ 10^{-7} + 10\ 10^{-7}\ sin(\phi); \quad I = 0.5\ sin(\phi/2) \tag{6.12}$$

The wavelength λ is in nm and the intensity I in units of 10^{13} W/cm^2. The angle ϕ goes from 0 to 2π. The loop goes around the EP with coordinates in the (intensity, wavelength) control plane estimated to be $\lambda = 255.25$ nm and $I = 0.395\ 10^{13}$ W/cm^2 for the pair $8 - 9$. The state 8 is finally reached. This is shown in Figure (6.7). We also demonstrate that this transfer is robust, *i. e.*it still holds when adding further channels to the basic two-channel model. Convergence is reached when, as displayed in Figure (6.7), one Floquet block is added on both sides of the reference block, that is the block of the single-photon two-channel model. However near-convergence is already obtained with only the block above the reference block included. This shows incidentally that in all these calculations the EP is still within the loop.

Another important consequence of the occurrence of exceptional points is that on the EP the wavefunctions of the two resonances merge into a single one. This is illustrated in Figure (6.8) where the wavefunctions issued from 8 and 9 are shown (in dashed and in thin solid lines respectively) at two different intensities for a wavelength $\lambda = 442.26$ nm. When the intensity is rather low

($I = 0.05\ 10^{13}$ W/cm^2), the nodal structure in the lower channel (g) is still recognizable. The resonance energies are then respectively $-6849.89 - i\ 9.21$ cm^{-1} and $-5626.68 - i\ 68.06$ cm^{-1}. For an intensity close to that of the EP, $I = 0.3949\ 10^{13}$ W/cm^2, for which the resonance energies are still distinguishable and are $-5926.52 - i\ 391.58$ cm^{-1} and $-5917.11 - i\ 399.21$, the two wavefunctions become almost undistinguishable. A very interesting feature, the self-orthogonality phenomenon, occurs whenever two photodissociation resonances coalesce. This can numerically be evidenced from the so-called self-overlap σ of a given resonance solution $\Psi(R,t)$ evaluated as [27]:

$$\sigma = \sum_{n=-\infty}^{n=+\infty} \int_0^\infty dR \left[\left(\psi_{g,n}(R)\right)^2 + \left(\psi_{u,n}(R)\right)^2 \right] \quad . \tag{6.13}$$

It is important to note that no complex conjugate of the Floquet components $\psi_{g,u}(R)$ appears here in the implied scalar-product, consistently with the definition of the non-hermitian c-product (see Ref. [73, 74]). The self-orthogonality phenomenon cannot be described using the standard hermitian definition where the usual complex conjugates of $\psi_{g,u}(R)$ would appear. The corresponding values are given in Figure (6.7) where one observes a significant decrease of σ_8 and σ_9 near the EP.

The occurence of Zero Width Resonances and of Exceptional Points in the context of laser-induced photodissociation can be exploited in various ways. We have shown how Zero-Width Resonances can be beneficial in purification scenarios. We have also shown that Exceptional Points can be exploited in vibrational transfer scenarios. Such scenarios could ultimately be applied for vibrational cooling strategies by depleting all vibrational levels except the ground ($v = 0$) one.

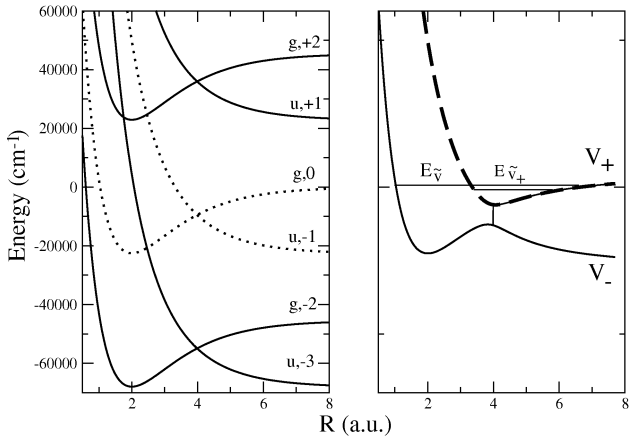

Figure 6.1: Diabatic (left panel) and adiabatic (right panel) potentials of H_2^+ for a wavelength $\lambda = 440$ nm and a field intensity 10^{13} W/cm^2. The excited state potential has been lowered by $\hbar\omega$. $E_{\tilde{v}}$ and E_{v_+} are representative of energies associated with the modified diabatic and the modified upper adiabatic potentials respectively.

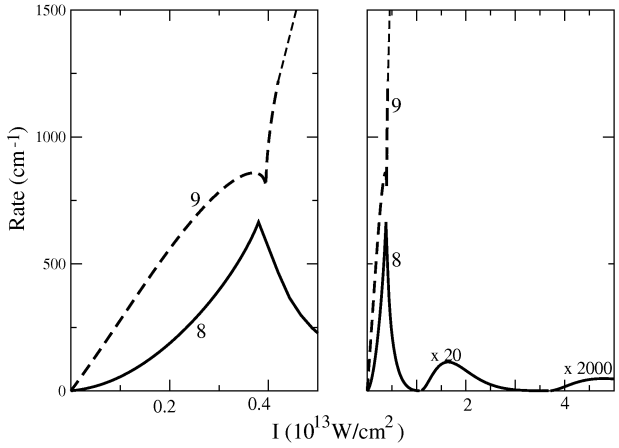

Figure 6.2: The rates versus intensity for the resonances issued from the vibrational states $v = 8$ and $v = 9$ for a wavelength $\lambda = 255.255$ nm. Th left panel zooms the region showing how the rates approach each other for an intensity $I = 0.395\ 10^{13}$ W/cm^2. The rigth panel shows that at two intensities the rate passes through a zero value. An amplification is needed because when the intensity increases, the coupling between the two adiabatic potential decreases and the bound states of the upper adiabatic potential become very good approximations.

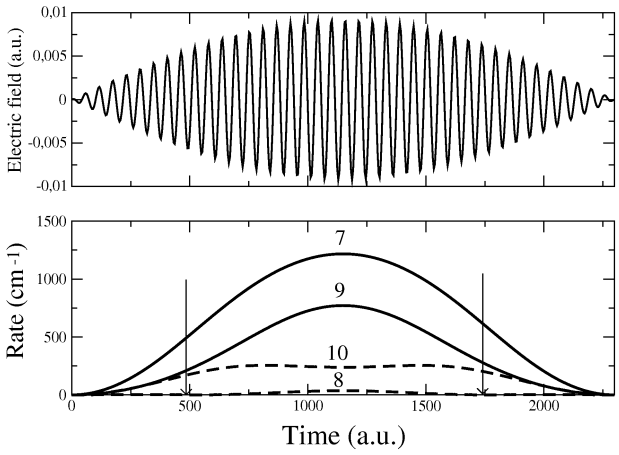

Figure 6.3: Time variation of the rates of various resonances followed adiabatically during the pulse shown in the upper panel. The wavelength is $\lambda = 420$ nm. The mid-pulse intensity $I = 0.3\ 10^{13}$ W/cm^2 is large enough for the width of the resonance $v = 8$ to pass twice through a null value at times depicted by the vertical arrows of the lower panel, but not large enough for resonance $v = 10$ to reach a zero width. Resonances $v = 7$ and $v = 9$ belong to the class reaching high values of the rates because of their shape nature.

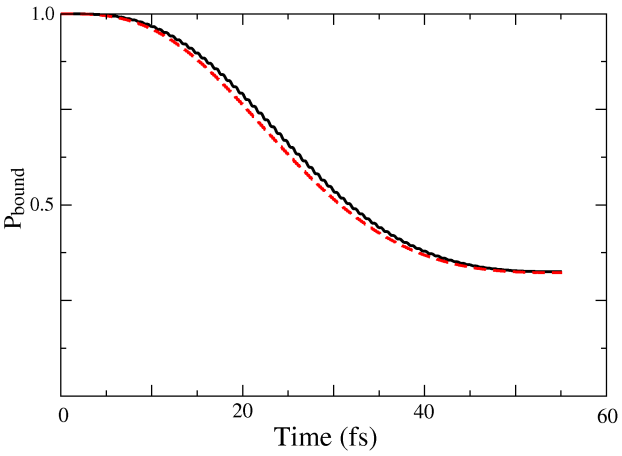

Figure 6.4: Time variation of the probability to remain bound for the resonance labelled $v = 7$. The wavelength is $\lambda = 420$ nm. The mid-pulse intensity is $I = 0.05 \times 10^{13}$ W/cm^2. The pulse duration is 56 fs. The dashed curve is for the adiabatic Floquet treatment while the solid curve is for the time-dependent calculation.

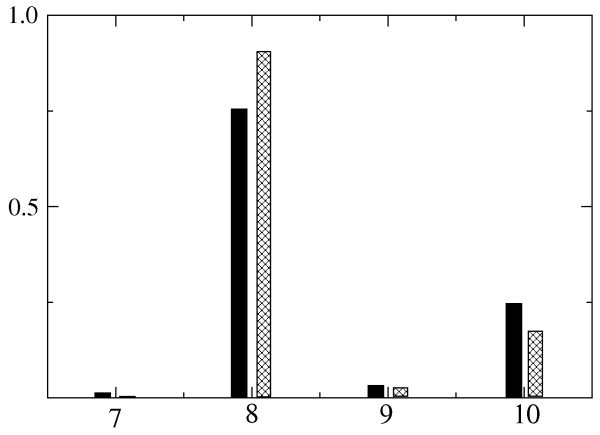

Figure 6.5: Comparison of survival probabilities for the resonances 7 to 10 calculated either from a time-dependent wave packet propagation or from the adiabatic Floquet formalism with the same laser parameters as in Figure (6.3) and for a light pulse duration of t_f = 56 fs, corresponding to about 40 optical cycles. For each initial state, the wave packet propagation result is given by the left histograms (full boxes), while the adiabatic Floquet result is represented by the right histograms (hatched boxes). Only the state 8 shows a large survival probability because, as shown on Figure (6.3), its rate passes twice through a null value.

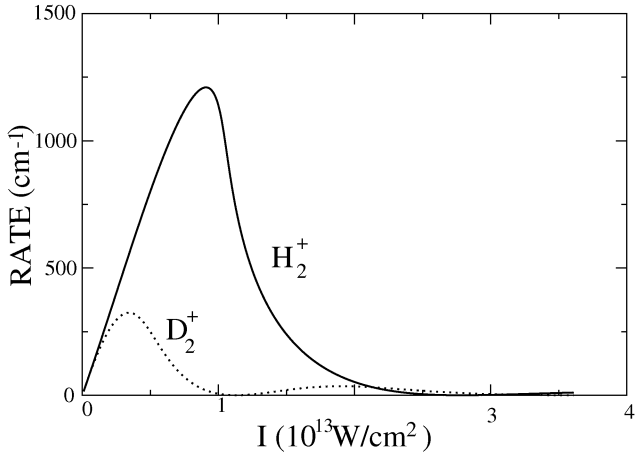

Figure 6.6: Rates as a function of laser intensity for D_2^+ (dotted line) and H_2^+ (solid line). The laser wavelength is taken as 120 nm and the resonance under consideration is v=2

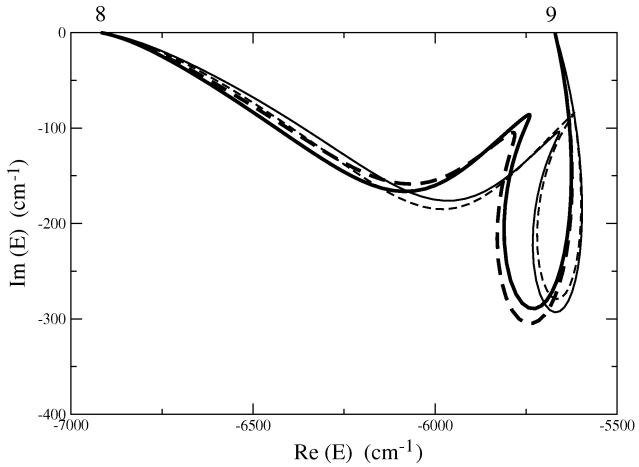

Figure 6.7: Transfer from state 9 to state 8 when following adiabatically the resonance issued from 9 around the exceptional point where the resonances energies from 8 and 9 are merging. The paths are as follows: thin solid curve, the 2-channel model; thin dashed curve, 4 channels, with inclusion of the two lower channels of Figure (6.1); thick dashed curve, 4 channels, with inclusion of the two higher channels of Figure (6.1); thick solid curve, 6 channels, with inclusion of all channels of Figure (6.1).

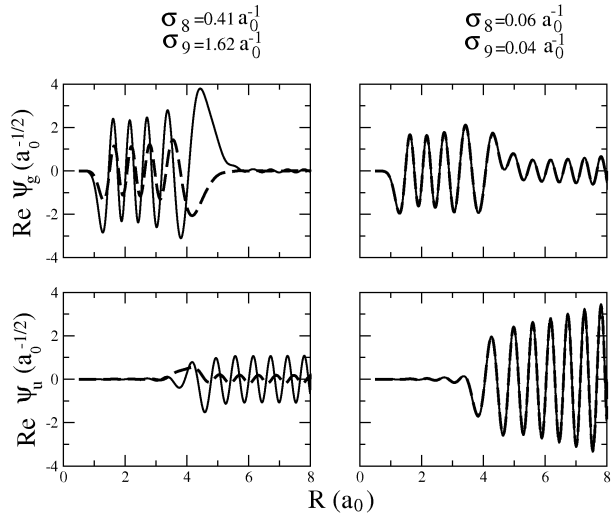

Figure 6.8: The resonance wave functions and their corresponding self-overlaps at two different intensities $I = 0.05\ 10^{13}$ W/cm^2 (left panels) and $I = 0.3949\ 10^{13}$ W/cm^2 (right panels). Only the real part of each channel wave function is displayed.

7. Conclusion

Intense laser-induced molecular dissociation is definitely one of the most challenging applications of Quantum Mechanics where theoretical models and their computer-based numerical simulations may help in a quantitative understanding and prediction of experimental discoveries. This has been exemplified in this review on some simple systems. Although the low-dimensional models considered may appear limited, the nature and dynamics of the unstable states (resonances) and the basic mechanisms associated with them are of wider application range than evoked, and particularly in reactivity control. Strong field mechanisms, specifically barrier suppression and dynamical quenching in the IR regime or bond softening and vibrational trapping in the UV regime, are basic tools for a detailed interpretation of experimental observations made on ATD spectra. By adjusting adequately the laser's characteristics such as its intensity, frequency, polarization, pulse shape and phase, one can bring into competition chemical bond softening and/or hardening mechanisms, to obtain intense laser control scenarios of photochemical processes. Advantage can be taken of such a competition to direct the chemical reaction towards a given channel, involving the breaking of a given bond, while the others are stabilized by laser-induced trapping or quenching mechanisms.

It is important to note that control strategies based on resonances and basic mechanisms present interesting complementarities when compared to optimal control schemes, with the advantage for the formers of a thorough understanding of the dynamics on one hand, and robustness and transposability, on the other hand. More precisely, this complementarity can be discussed referring to three observations: (i) there is no single solution arising from optimal control scenarios (not only different criteria, but also different sampling spaces for the laser parameters to be optimized would lead to different results); (ii) a careful study of the laser-induced dynamics can help to the identification (or guess) of some basic mechanisms leading to the desired observable in a very robust way (not a black-box numerical approach); (iii) by appropriately building the

targets and delineating the parameter sampling space, we can help the optimal control scheme to take advantage of the mechanisms and specific behaviors of the resonances. Finally, we emphasize again that we refer to basic mechanisms or resonances only for interpretation or control purposes, or when describing strictly time-adiabatic processes, all calculations dealing with the "exact" resolution of the time-dependent Schrdinger equation.

The opposition of sudden excitations and adiabatic dynamics provides other ways of controlling and/or imaging dissociative ionization processes. This has been illustrated by quantitative theoretical interpretations of observations made in the XUV + IR pump-probe experiment discussed in section 5, where the imaging and/or possible dynamical control of the dissociative ionization of H_2 rest on a partial breakdown of the widely common assumption of adiabatic transports of individual, isolated resonances during the laser-induced dynamics. On the other hand, it is rather within such an adiabatic regime, associated with a long pulse duration, that one encounters counterintuitive situations due to highly non-linear behaviors in the transports and decays of single resonances induced by strong fields as exemplified by ZWRs, denoting situations where a molecule irradiated by a very strong field is stabilized with respect to dissociation. Advantage can be taken from a ZWR that is adiabatically connected with a given field-free vibrational state, as one can manage to bring all population in other vibrational states to dissociation, leaving residual bound population in the ZWR under consideration: This constitutes a vibrational purification control scheme. In the same spirit, it is possible to proceed to a separation of different chemical species (two isotopes, for instance) in a mixture merely by dissociating certain species while stabilizing others through a ZWR reached within the same laser excitation, the result being an enrichment of the mixture in the stabilized species.

At the frontier of non-adiabaticity (*i. e.* of the breakdown of the single resonance adiabatic transport approximation) lie the EPs that can be reached by an appropriate combination of laser parameters (frequency and intensity). A coalescence of two resonances adiabatically connected with two different field-

free vibrational states occurs at an EP. With a loop in the (frequency, intensity) plane encircling the EP, such a resonance coalescence situation is produced. As the loop is followed adiabatically, the system switches from a single resonance connected with a given vibrational level to a second resonance, and ends up in a final, different vibrational level when the laser is turned off: This is a vibrational transfer control scheme. Combining ZWRs and EPs and using appropriately chirped laser pulses, it is easily realized how a molecular cooling control objective can be attained by depleting all vibrational levels except the ground (v=0) one.

An important issue concerns the robustness of the control strategies discussed presently with respect to the introduction of rotational degrees of freedom and additional electronic states. We have not addressed this issue explicitly here, but studies have been made, e.g. on rotational effects on the existence of ZWRs, and give reassuring results[6]. Even if there may be some efficiency loss upon inclusion of further channels in the model, the general strategies seem to resist to these additional degrees of freedom. Laser-induced molecular orientation, manipulation and imaging are among the future goals of such control schemes based on laser-induced resonances and associated processes.

Acknowledgments

Financial support by the Natural Sciences and Engineering Research Council of Canada (NSERC) in the form of research grants to TTND is gratefully acknowledged. We thank M. Peters for lending a helping hand in the preparation of the manuscript.

[1] A. D. Bandrauk, Quantum and Semiclassical Electrodynamics in *Molecules in Laser Fields*, A. D. Bandrauk, ed., M. Dekker publ., New-York, 1994.

[2] A. D. Bandrauk, E. E. Aubanel, J. M. Gauthier, Theory of Molecules in Intense Laser Fields in *Molecules in Laser Fields*, Dekker, New York, 1994.

[3] A. Giusti-Suzor, X. He, O. Atabek, F. H. Mies, *Above-threshold dissociation of H_2^+ in intense laser fields*, Phys. Rev. Lett. 64 (1990) 515.

[4] O. Atabek, R. Lefebvre, T. T. NguyenDang, Control Theory and Quantum Dynamics in *Handbook of Numerical Analysis* T. G. Ciarlet, J. L. Lyons and C. Lebris, ed., Vol. X, Elsevier, 2003.

[5] C. Lefebvre, T. T. Nguyen-Dang, O. Atabek, Phys. Rev. A 75 (2007) 023404.

[6] O. Atabek, R. Lefebvre, C. Lefebvre, T. T. Nguyen-Dang, Phys. Rev. A 77 (2008) 043413.

[7] A. F. J. Siegert, Phys. Rev. 56 (1939) 750.

[8] L. Fox, E. T. Goodwin, Phil. Trans. Royal Soc., London 245 (1953) 1.

[9] S. I. Chu, Adv. Chem. Phys. LXIII (1989) 739.

[10] F. Châteauneuf, T. T. Nguyen-Dang, N. Ouellet, O. Atabek, J. Chem. Phys. 108 (1998) 3974.

[11] H. Abou-Rachid, T. T. Nguyen-Dang, O. Atabek., J. Chem. Phys. 110 (1999) 4737.

[12] H. Abou-Rachid, T. Nguyen-Dang, O. Atabek, J. Chem. Phys. 114 (2001) 2197.

[13] H. Niikura, P. B. Corkum, D. M. Villeneuve, Phys. Rev. Lett. 90 (2003) 203601.

[14] O. Atabek, R. Lefebvre, F. X. Gadéa, Phys. Rev. A 74 (2006) 063412.

[15] T. Kato, J. Phys .Soc. Jpn 5 (1958) 435.

[16] O. Atabek, R. Lefebvre, J. Phys. Chem., 114 (2010) 3031

[17] F. H. M. Faisal, Theory of Multiphoton Processes, Plenum, New-York, 1986.

[18] H. R. Reiss, Phys. Rev. A 22 (1980) 1786.

[19] C. Cohen-Tannoudji, J. Dupont-Roc, G. Grynberg, Atom-Photon Interactions, Wiley-Interscience, 1992.

[20] M. Born, R. Oppenheimer, Ann. Physik 84 (1927) 457.

[21] G. Floquet, Ann. de l'Ecol. Norm. Sup. 12 (1883) 47.

[22] N. Moiseyev, Phys. Reports 302 (1998) 211.

[23] M. D. Feit, J. A. Fleck, A. Steiger, J. Comp. Phys. 47 (1982) 410.

[24] A. Keller, Phys. Rev. A 52 (1995) 1450.

[25] F. Kelkensberg, C. Lefebvre, W. Siu, O. Ghafur, T. T. Nguyen-Dang, O. Atabek, A. Keller, V. Serov, P. Johnsson, M. Swoboda, T. Remetter, A. L'Huillier, S. Zherebtsov, G. Sansone, E. Benedetti, F. Ferrari, M. Nisoli, F. Lépine, M. F. Kling, M. J. J. Vrakking, Phys. Rev. Lett. 103 (2009) 123005.

[26] C. Lefebvre, Stratégies de contrôle laser de la dynamique moléculaire, Ph. D. thesis, Université Laval, Québec, and Université Paris-sud 11, Orsay, 2008.

[27] R. Lefebvre, O. Atabek, M. Šindelka, N. Moiseyev, Phys. Rev. Lett. 103 (2009) 123003.

[28] S. Chelkowski, T. Zuo, O. Atabek, A. D. Bandrauk, Phys. Rev. A 52 (1995) 2977.

[29] S. Guérin, F. Monti, J. M. Dupont, H. Jauslin, J. Phys.A: Math. Gen. 30 (1997) 7193.

[30] S. Guérin, H. R. Jauslin, Adv. Chem. Phys. 125 (2003) 1.

[31] U. Peskin, N. Moiseyev, J. Chem. Phys. 99 (1993) 4590.

[32] N. Moiseyev, M. Chrysos, R. Lefebvre, J. Phys. B: At. Mol. Opt. Phys. 28 (1995) 2599.

[33] N. Moiseyev, O. E. Alon, V. Ryabov, J. Phys. B: At. Mol. Opt. Phys. 28 (1995) 2611.

[34] C. Kittel, Introduction to Solid State Physics, 7th Edition, John Wiley, New-York, 1996.

[35] J. M. Okuniewickz, J. Math. Phys. 15 (1974) 1587.

[36] T. T. Nguyen-Dang, F. Châteauneuf, O. Atabek, X. He, Phys. Rev. A 51 (1995) 1387.

[37] T. Kato, Journ. Phys. Soc. Jap. 5 (1950) 435.

[38] H. P. Breuer, K. Dietz, M. Holthaus, Phys. Rev. A 47 (1993) 725.

[39] H. P. Breuer, M. Holthaus, J. Phys. Chem. 97 (1993) 12634.

[40] T. T. Nguyen-Dang, E. Sinelnikov, A. Keller, O. Atabek, Phys. Rev. A 76 (2007) 052118.

[41] F. Châteauneuf, Dynamique et structure moléculaire en champs laser intenses, Ph. D. thesis, Département de chimie, Université Laval, 1997.

[42] C. A. Nicolaides, D. R. Beck, Phys. Lett. A 65 (1978) 11.

[43] B. Simon, Phys. Lett. A 71 (1979) 211.

[44] D. W. Norcross, M. J. Seaton, J. Phys. B 6 (1973) 614.

[45] C. E. Dateo, H. Metiu, J. Chem. Phys. 95 (1991) 7392.

[46] R. Kosloff, J. Phys. Chem. 92 (1988) 2087.

[47] D. J. Kouri, R. C. Mowrey, J. Chem Phys. 80 (1987) 2578.

[48] R. Heather, H. Metiu, J. Chem. Phys. 86 (1987) 5009.

[49] R. Numico, A. Keller, O. Atabek, Phys. Rev. A 52 (1995) 1298.

[50] A. Zavriyev, P. H. Bucksbaum, H. G. Muller, D. W. Schumacher, Phys. Rev. A 42 (1990) 5500.

[51] G. Jolicard, O. Atabek, Phys. Rev. A 46 (1992) 5845.

[52] G. Jolicard, J. P. Killingbeck, D. Viennot, J. Buldyreva, P. Joubert, J. Phys. A 41 (2008) 095303.

[53] G. Yao, S. I. Chu, Phys. Rev. A 48 (1993) 485.

[54] E. E. Aubanel, A. Conjusteau, A. D. Bandrauk, Phys. Rev. A 48 (1993) R4011.

[55] O. Atabek, M. Chrysos, R. Lefebvre, Phys. Rev. A 49 (1994) R8.

[56] R. Numico, A. Keller, O. Atabek, Phys. Rev. A 56 (1997) 772.

[57] A. D. Bandrauk, M. S. Child, Mol. Phys. 19 (1970) 95.

[58] O. Atabek, M. Chrysos, R. Lefebvre, Phys. Rev. A 49 (1994) R8.

[59] A. H. Zewail, J. of Phys. Chem. A 104 (2000) 5660.

[60] P. B. Corkum, F. Krausz, H. Ferenc, Nat. Phys. 3 (2006) 381.

[61] M. Drescher, M. Hentschel, R. Kienberger, G. Tempea, C. Spielmann, G. A. Reider, P. B. Corkum, F. Krausz, Science 291 (5510) (2001) 1923.

[62] C. C. Chirila, M. Lein, Phys. Rev. A 77 (4) (2008) 043403.

[63] T. T. Nguyen-Dang, F. Châteauneuf, S. Manoli, O. Atabek, A. Keller, Phys. Rev. A 56 (1997) 2142.

[64] V. Serov, A. Keller, O. Atabek, H. Figger, D. Pavicic, Phys. Rev. A 72 (3) (2005) 033413.

[65] K. Sändig, H. Figger, T. W. Hänsch, Phys. Rev. Lett. 85 (23) (2000) 4876.

[66] C. Dembowski, F. Gräf, H. L. Harney, A. Heine, W. D. Heiss, H. Rehfeld, A. Richter, Phys. Rev. Lett. 86 (2001) 787.

[67] T. Stehmann, W. D. Heiss, F. G. Scholtz, J. Phys. A:Math. Gen. 37 (2004) 7813.

[68] E. Navericius, N. Moiseyev, Phys. Rev. Lett. 84 (2000) 1681.

[69] H. Cartarius, J. Main, G. Wunner, Phys. Rev. Lett. 99 (2007) 173003.

[70] M. S. Child, Mol. Phys. 32 (1976) 1495.

[71] O. Atabek, R. Lefebvre, Phys. Rev. A 78 (2008) 043419.

[72] R. Lefebvre, O. Atabek, Eur. J. Phys. D, 56 (2010) 317.

[73] N. Moiseyev, Phys. Rep. 302 (1998) 212.

[74] N. Moiseyev, P. R. Certain, F. Weinhold, Mol. Phys. 36 (1978) 1613.